論文 / 著書情報
Article / Book Information

題目(和文)	
Title(English)	Lattice Deformation and Elastic State Associated with F.C.C. to B.C.C. Martensitic Transformation in Iron Alloys
著者(和文)	加藤雅治
Author(English)	MASAHARU KATO
出典(和文)	学位:工学博士, 学位授与機関:東京工業大学, 報告番号:甲第962号, 授与年月日:1978年3月26日, 学位の種別:課程博士, 審査員:
Citation(English)	Degree:Doctor of Engineering, Conferring organization: Tokyo Institute of Technology, Report number:甲第962号, Conferred date:1978/3/26, Degree Type:Course doctor, Examiner:
学位種別(和文)	博士論文
Type(English)	Doctoral Thesis

TOKYO INSTITUTE OF TECHNOLOGY

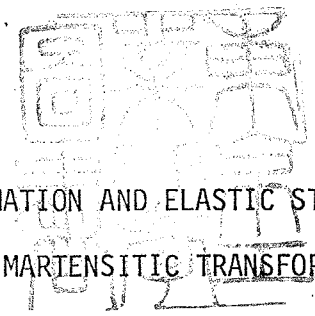

LATTICE DEFORMATION AND ELASTIC STATE ASSOCIATED WITH F.C.C. TO B.C.C. MARTENSITIC TRANSFORMATION IN IRON ALLOYS

A DISSERTATION

for the degree

DOCTOR OF ENGINEERING

Field of Metallurgical Engineering

by

MASAHARU KATO

Ookayama

Meguro-ku

Tokyo, Japan

1978

CONTENTS

CHAPTER 1

INTRODUCTION

Martensitic transformations are characterized by the cooperative shear movement of atoms and by the existence of orientation relationships between the parent phase and the martensite. These characteristics enable one to suppose that the occurrence of a particular type of martensitic transformation is related to the operation of a particular shear system. From this, one can further expect that if stress is applied during the transformation, a variant of martensite, usually identified as a stress-induced martensite with a certain crystallographic orientation to the parent phase, will be formed preferentially, depending on the direction and sense of the applied stress.

Several experimental studies have been reported which have examined the above expectation with respect to F.C.C. to B.C.C. martensitic transformation in single crystals; an Fe-Ni alloy by Bogers[1], thin films of Fe by Olsen and Jesser[2], and stainless steels by Higo et al[3] and Stone and Thomas[4].

However, the shear deformation accompanying a martensitic transformation is, in a sense, vaguely defined. It may be taken as the shear movement of atoms to change the lattice on an atomic scale or as the macroscopic shear deformation such as a component of the shape deformation discussed in the phenomenological crystallographic theory[5,6] of martensitic transformations.

Historically speaking, the first rational explanation of the stress effect on nucleation of martensite was offered by Patel and Cohen[7]. They suggested that the applied stress aided the total shape deformation accompanying the transformation. Subsequently, Christian considered that the preferential formation of the specific martensite variants is determined by the interaction between applied stress and the shape deformation discussed in the phenomenological theory[8].

However, the thermodynamic discussion such as that by Patel and Cohen and the phenomenological theory do not necessarily go together with each other. For, in the former, necessity of some activation process arises essentially from considering the elastic and interface energies accompanying the transformation, while, in the latter, total shape deformation is considered to occur in such a manner that the elastic energy becomes zero and, moreover, interface energy is neglected. Thus, it is doubtful that one could duly understand the stress effect on the martensitic transformation in terms of the total shape deformation.

Although Patel and Cohen's idea has been utilized by several workers,

unambiguous and conclusive experimental evidence to support the idea has not been offered yet. For example, Stone and Thomas discussed the stress effect on the transformation in a stainless steel in terms of the assumption by Patel and Cohen and could not explain the experimental results completely[4]. Though the experimental results are not clearly presented because of the use of polycrystalline specimens, an analysis is along this direction in some studies[9-11].

The second idea is just the use of the total lattice (Bain) deformation. This approach was taken by Olsen and Jesser[12] to examine the preferential formation of some particular variants of martensite in iron films which had originally been grown epitaxially on copper or nickel substrates and had been under stress caused by the difference of the lattice parameters between iron films and substrates[2]. Olsen and Jesser discussed the experimental observation in terms of the interaction between the stress and the Bain deformation together with the operation of some shear systems, which are the main concern of the present study. One notes that the study by Olsen and Jesser has an advantage as well as a disadvantage. Both of these are direct consequences of the experimental condition; thin films and, at the same time, restricted choices of materials and stress systems.

Thirdly, an idea that the applied stress aids the shear deformation, which can be considered as the further factorization of the lattice deformation, was developed by Bogers and Burgers[13]. They explained the observed results by Bogers[1] by introducing two $\{111\}_f\langle 211\rangle_f$ shear systems which are the main components of the Bain deformation. Stress-induced martensites observed by Bogers were the ones which were formed under the $[001]_f$ or $[110]_f$ compressive loading. As the first attempt to examine a stress effect in a single crystal, the work by Bogers should remain to be a milestone in the history of the study of martensitic transformation. However, shear systems which convert the parent phase lattice to the martensite lattice are usually of less symmetric character. Thus, it is sometimes more preferable to use less symmetric crystal direction as a stress axis than the highly symmetric ones which were adopted by Bogers.

The experiment on this standpoint was carried out by Higo et al in an 18-14 stainless steel single crystal[3]. They investigated ε- and α-martensites which had been formed under asymmetrical tensile and compressive loadings and concluded that the applied stress aids the $\{111\}_f\langle 211\rangle_f$ shear system in the $\gamma \rightarrow \alpha$ lattice change. In a stainless steel, ε- and α-martensites coexist in some temperature ranges, whether or not the formation of the two types of

martensite is related to each other. For this reason, if we are only interested in the $\gamma \rightarrow \alpha$ transformation, it may be more natural and direct to investigate alloys in which only a $\gamma \rightarrow \alpha$ transformation occurs. In addition, such a study will shed light on the lonely study by Higo et al belonging to a minority group in the world of martensitic transformation study.

Motivated, intrigued and encouraged by the above mentioned current state of understanding about stress effect on martensitic transformation, the present study was started. First, effect of the applied stress on the F.C.C. to B.C.C. martensitic transformation was examined. The alloys used in the experiment were Fe-23Ni-5Cr and Cu-1.06Fe single crystals. In the former, needle-like surface martensite was formed, while in the latter, spherical γ-iron precipitates surrounded by the copper matrix transform into α-iron martensite. If applied stress aids the total shape deformation in the transformation, the stress-induced martensite variants in these two alloys must be different in each other even if the stress is applied along the same direction. For, the shape deformation of martensite in an Fe-23Ni-5Cr alloy is entirely different from that in a Cu-1.06Fe alloy.

On the other hand, if the deformation in the lattice change is aided by the applied stress, the variants formed will essentially be identical for these two alloys. Therefore, by examining the martensite in these two alloys, one will get the straightforward answer to the question, " In which stage of the transformation should the stress effect appear? "

The $\gamma \rightarrow \alpha$ transformation has also been a good object in the phenomenological crystallographic theory[5,6]. This is because it is not so simple as the $\gamma \rightarrow \varepsilon$ transformation and it is widely observed in many ferrous alloys. The phenomenological theory was born when the understanding of the irrational habit plane and orientation relationship found in ferrous martensite was needed. It is characterized by the consideration of the invariant lattice deformation based on a certain criterion, ' Invariant Plane Deformation '. Nowadays, it has been expanded by postulating two or more lattice invariant deformations[14,15] or by introducing a dilatation parameter[16]. However, such modifications of the original phenomenological theory result in the increase in the number of arbitrary parameters. Is it along right direction in understanding physics involved that a number of arbitrary parameters are chosen to match a calculation with an experimental observation? The answer will, of course, depend on individuals. However, the present study takes the attitude to say, "No", to this question, although it cannot be denied that the majority in the research world of martensitic transformation will follow the

phenomenological theory.

Therefore, the present study will examine the physical meaning of the criterion (Invariant Plane Deformation) with the infinitesimal deformation theory, which enables one to compute the elastic state and the elastic energy associated with the deformation involving the transformation and the plastic deformation. From this, some interesting facts, which have been overlooked until now, will be pointed out. A few more words before concluding this paragraph. Spherical iron particles in copper do not have a shape which is within the treatment of the phenomenological theory.

Thus, the elastic calculations will be fully utilized to examine the elastic state and the elastic energy of the martensite formed from spherical particles. In addition, a disc-shaped martensite will be treated similarly. These calculations were based on the recent study by Mura et al[17], on the ellipsoidal inclusion with eigenstrains. Historically speaking, the elastic state of the ellipsoidal inclusion was first studied by Eshelby[18,19]. Mura et al's work belongs to the developments of Eshelby's theory. The papers by Kinoshita and Mura[20] and Mura and Cheng[21] are also in this category and will be utilized to discuss some experimental observations in this study.

This thesis goes as follows:

In Chapter 2, stress-induced martensite formed in Fe-23Ni-5Cr single crystals is examined. Experimental results are well-explained by the assumption that the applied stress aids the $\{111\}_f\langle 211\rangle_f$ shear system in the lattice change during the transformation.

In Chapter 3, the elastic calculation in an ellipsoidal inclusion with periodically distributed eigenstrains is applied to the evaluation of the elastic energy with disc and spherical martensites. The significant contribution of the periodically distributed eigenstrain, which has been, until now, overlooked in the phenomenological calculation, is found to be very important in the energetics involved in martensitic transformations.

In Chapter 4, a spherical iron martensite induced by the applied stress in a Cu-1.06Fe alloy single crystal is examined. Together with the results in Chapter 2, it is concluded that the applied stress aids the $\{111\}_f\langle 211\rangle_f$ shear deformation in the initial stage of the transformation. In addition, by applying the calculated results in Chapter 3, specific twin-interface energy in the α-iron is evaluated.

In Chapter 5, orientation and shape dependence of the elastic energy associated with precipitation is considered in anisotropic media. This study has been motivated by the spherical shape of iron particles formed by the

precipitation in Cu-Fe alloys. Depending on alloys, the precipitates with the transformation strain of pure dilatation (hydrostatic) components take a disc or spherical shape. There must be a reason, of energetics character, to account for the observed shape of the precipitates. The shape dependence of the elastic energy is further examined in the light of the interaction between the elements constituting a precipitate.

In Chapter 6, the total summary of this thesis and the concluding remarks are given.

CHAPTER 2

STRESS-INDUCED MARTENSITE IN Fe-23Ni-5Cr ALLOY SINGLE CRYSTALS

2-1. Motivation of the Study

Martensitic transformation without or under stress in Fe-Ni or Fe-Ni-Cr alloys has been extensively examined by many investigators. This is because morphology and structure of martensite in these alloys are very similar to those found in the industrial ferrous alloys and, moreover, one can easily change the temperature to start transformation (Ms temperature) by changing the nickel content. In the present work, single crystals of an Fe-23Ni-5Cr alloy were used. This alloy consists of the paramagnetic γ-austenite (F.C.C.) in room temperature, while by cooling down to the lower temperatures it transforms into ferromagnetic α-martensite (B.C.C.).

Some experimental works on the examination of the relation between applied stress and F.C.C. to B.C.C. martensitic transformation have been reported. However, most were done by using the polycrystalline specimens. It is surprising that there have been only a few works done with single crystal specimens; an Fe-Ni alloy by Bogers[1], thin films of Fe by Olsen and Jesser[2], and stainless steels by Higo et al[3] and Stone and Thomas[4].

However, the experiment by Bogers was performed under the limited condition; he only observed the martensite which was formed under the symmetrical ($[001]_f$ and $[110]_f$) compressive loadings. Olsen and Jesser used thin films of Fe, which cannot necessarily be representative of bulk single crystals. Moreover, in stainless steels such as those utilized by Higo et al and Stone and Thomas, not only α- but also ε-martensite (H.C.P.) are formed, which makes the analysis of the experimental results complicated.

Furthermore, as has been related in Chapter 1, it has not yet been established that on which stage of the transformation the applied stress preferentially has an effect. Bogers and Burgers[13] discussed the experimental results by Bogers in terms of shear deformations to change the lattice. Olsen and Jesser[12] and Higo et al[3] followed a similar approach in examining their observations. Contrary to this, Stone and Thomas[4] discussed the stress-induced martensite in a stainless steel on the basis of the interaction between the total shape deformation of the transformation and the applied stress.

On the historical standpoint mentioned above, the emphasis in the present study is placed on the examination of the stress-induced $\gamma \rightarrow \alpha$ martensitic

transformation occurring under the symmetrical and asymmetrical tensile and compressive stresses in Fe-23Ni-5Cr single crystals.

2-2. Experimental Procedure

Three single crystals (crystals 1, 2 and 3) of an Fe-23.2wt%Ni-5.0wt%Cr alloy with less than 0.01wt%C were grown in alumina crucibles in vacuum by zone melting[22]. Presumably because of the inevitable segregation of alloying elements during zone melting, these three crystals differed with respect to their transformation characteristics on simple cooling. In crystal 1, a needle-like surface relief, approximately 10 × 200 μm, appeared at 253 K. Successive cooling to 77 K induced several surface reliefs. However, no burst formation of α-martensite occurred. In crystals 2 and 3, no surface relief appeared by cooling down to 77 K.

Rectangular flat specimens were cut from the single crystals using a wheel cutter. After removing the damaged surface layer by electrolytic polishing, these specimens were annealed under an argon atmosphere at 1273 K for 1 hour, water quenched and again electrolytically polished.

The orientation of the surface normals and the directions, along which the uniaxial stress was to be applied, were determined by the back-reflection Laue method and are shown in Fig.2.1. Crystals 1, 2 and 3 correspond to specimens with approximately $[729]_f$, $[427]_f$ and $[001]_f$ stress axes, respectively. The specimens were stressed either in tension or compression on an Instron-type testing machine at various temperatures with a strain rate of approximately 2×10^{-4} sec^{-1}. The gage lengths of the specimens were 20 mm in tension and 4 mm in compression and the cross section was 1 × 3 mm.

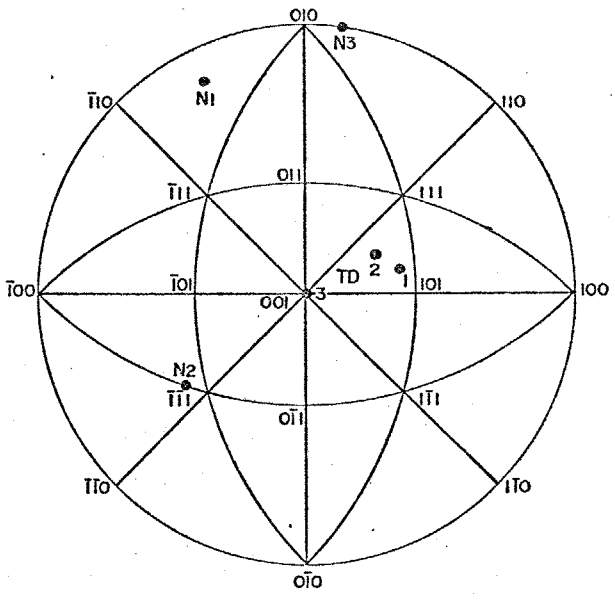

Fig.2.1
Stereographic projection showing the loading axes and flat surface normals in crystals 1, 2 and 3. TD and N represent the tensile (compressive) axes and the surface normals, respectively.

Optical microscopic observations were performed on the surface reliefs and on the martensite of the deformed specimens after polishing and etching. To determine the orientation relation-

ship of the variants of the stress-induced martensite to the parent phase, the X-ray Weissenberg method with the Kα line of Mo was applied to the samples. The samples for the X-ray analysis were prepared by mechanical polishing, spark cutting and electrolytical polishing out of the deformed specimens and were of approximately 2 × 2 × 0.1 mm sections.

2-3. Experimental Results

2-3-1. Stress-strain curves, deformation mode and transformation morphology

Stress-strain curves of crystal 1 (with $[729]_f$ stress axis) in tension and in compression are shown in Fig.2.2 ((a) and (b)). No serrated flow was observed at any temperature. The tensile tests were interrupted at every 5 % strain to examine the slip and transformation morphology. The arrow marks in Fig.2.2 indicate the strains at which the presence of the stress-induced martensite was first noted as surface relief under an optical microscope. In general, in crystals 1 and 2, specimens deformed in compression contained less martensites than those deformed in tension at the same temperature and the same strain. This point will be discussed later.

Figure 2.3 shows a sequence of martensite formation occurring simultaneously with slip during deformation at 195 K. It is noted that several martensite needles formed by simple cooling and shown in (a) did not grow on deformation. Contrary to this, as straining proceeded, the amount of the stress-induced martensite increased. Some martensites apparently showed growth on deformation in both lateral and lengthwise directions. However, the isothermal formation and growth of martensite were not observed.

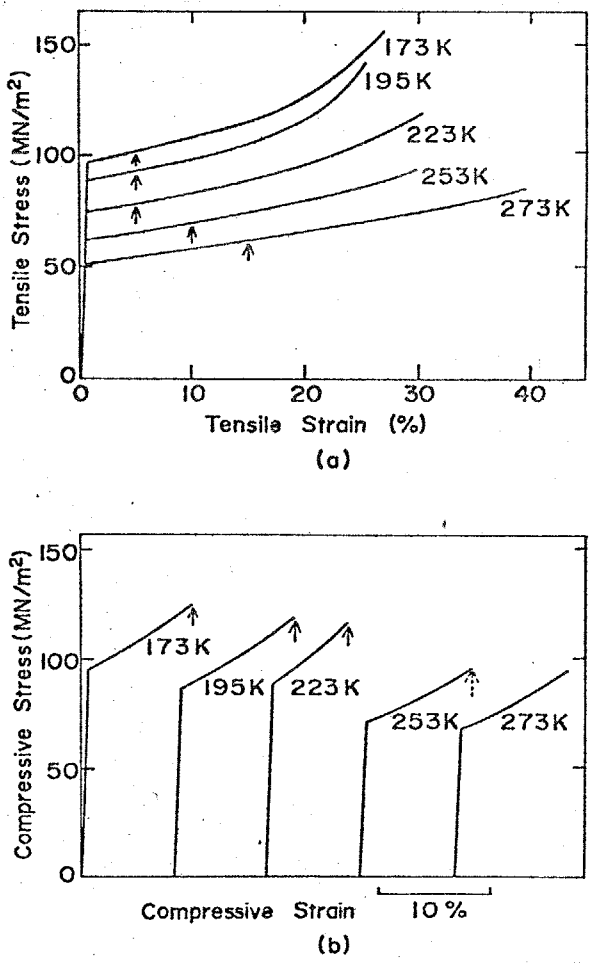

Fig.2.2

Tensile(a) and compressive(b) stress-strain curves of the specimens of crystal 1. Tensile tests were interrupted at every 5 % strain. Arrows indicate the strains at which the surface reliefs of stress-induced martensite were first noted. A dotted arrow in the compression at 253 K means that very few martensites were observed.

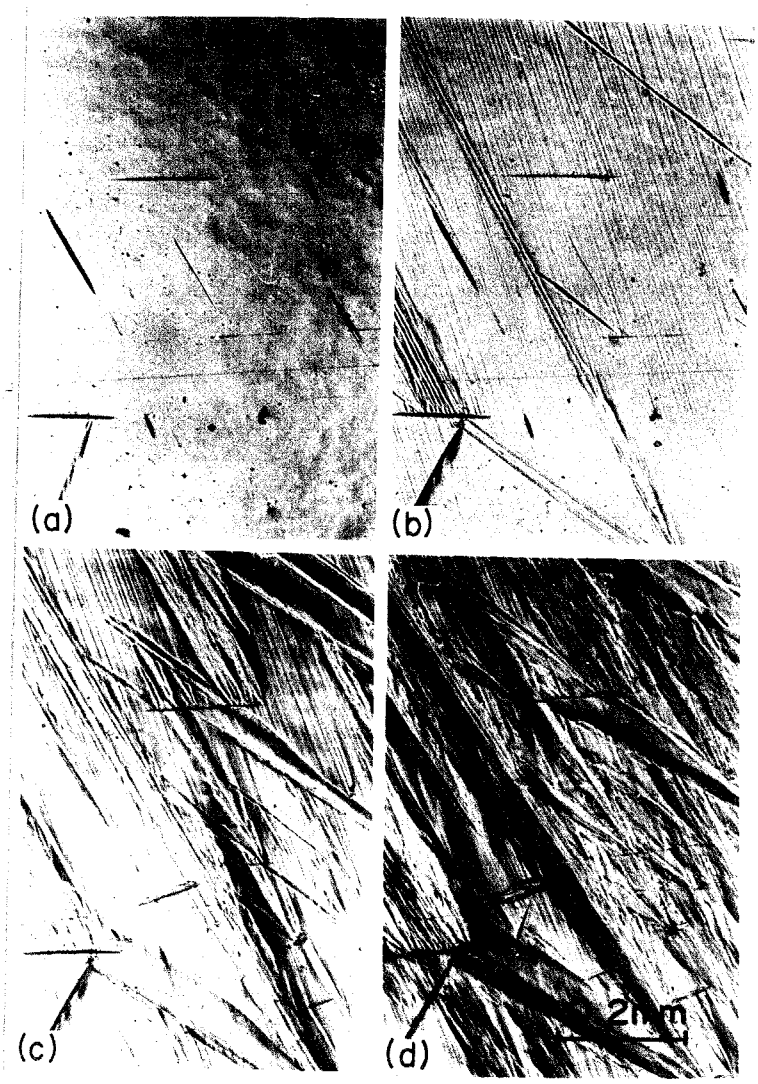

Fig.2.3

Optical micrographs showing the formation and growth of stress-induced martensite during tensile deformation at 195 K. Tensile strains are (a) 0 %, (b) 5 %, (c) 15 % and (d) 25 %.

From these reasons, the variants of martensite detected by the X-ray analysis were all identified as those which had been formed and grown under the applied stress. It can be seen from Fig.2.3 (b) and (c) that slip and transformation took place concurrently.

The lattice rotation accompanying the deformation was followed in every tensile test and a few compressive tests in crystals 1 and 2 by taking micro-Laue pictures from the γ-phase. The direction of straining calculated from the amount of strain under the assumption of single slip differed at most by only 2° from the observed strain axis. More significantly, the observed lattice rotation followed the arc expected from primary slip on the stereo-

graphic projection. This observation implies that the martensite did not occupy a significant volume of the specimen. This was supported by the optical microscopic observation of martensite, revealed by polishing and etching. The amount of martensite decreased as the depth from the original surface increased[23]. This fact indicates that the martensites formed during deformation are similar to the surface martensite reported by Klostermann and Burgers[24]. By using the linear traces which appeared as mid-rib and by conducting one surface analysis, it was found that all needles of the martensites lay parallel to the $\{211\}_f$ plane. This also agrees with the characteristics of the surface martensite[24].

Stress-strain curves in crystal 3 (with $[001]_f$ stress axis) are shown in Fig.2.4. Three specimens were deformed both in tension and in compression at 77 K in order to examine the reproducibility of deformation mode. Although the stress-strain curves were somewhat different among the specimens, the average critical resolved shear stress in crystal 3 was much higher than that in crystal 1, in which the specimens were deformed between 273 and 173 K. The small reproducibility in crystal 3 can be attributed to the unstable stress axis for slip, i.e., $[001]_f$. In all the specimens, stress-induced martensites were observed after the first 5 % strains. The morphology and the transformation mode of the stress-induced martensite were essentially identical to those in crystal 1. However, the most significant result in crystal 3 was that compressive loading induced more martensites than tensile loading, as shown in Fig.2.5. This result cannot be explained by the dilatation accompanying the $\gamma \rightarrow \alpha$ transformation and will be discussed later.

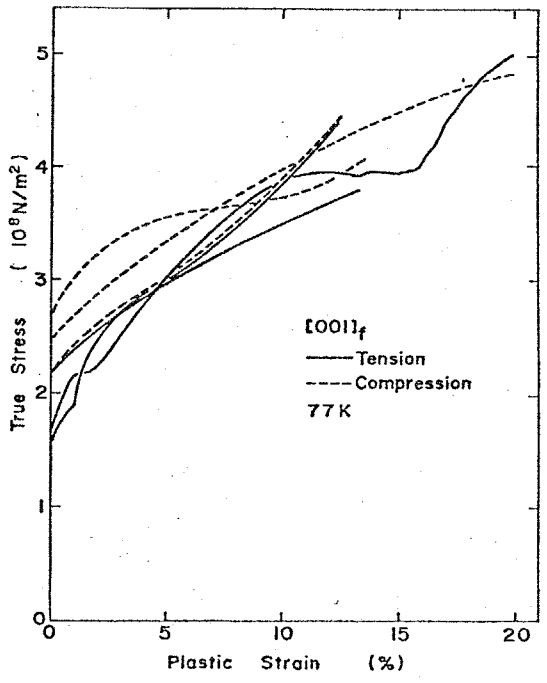

Fig.2.4

Stress-strain curves of crystal 3. Specimens were deformed along $[001]_f$ at 77 K.

2-3-2. Orientation of stress-induced martensite

Figure 2.6 shows an example of X-ray Weissenberg analysis. From this photograph, one can see that the $(110)_b$ plane of the martensite lies parallel to the $(111)_f$ plane of the parent phase and that the $[\bar{1}01]_f$ and $[1\bar{1}1]_b$

directions coincide with each other, showing the Kurdjumov-Sachs (K-S) orientation relationship. In this work, almost all the observed stress-induced martensites obeyed the K-S orientation relationship to the parent phase with one exception described later. For some variants in crystal 3, the precise determination of the orientation relationship was difficult because of the large deformation preceding the X-ray analysis. In such a case, the nearest

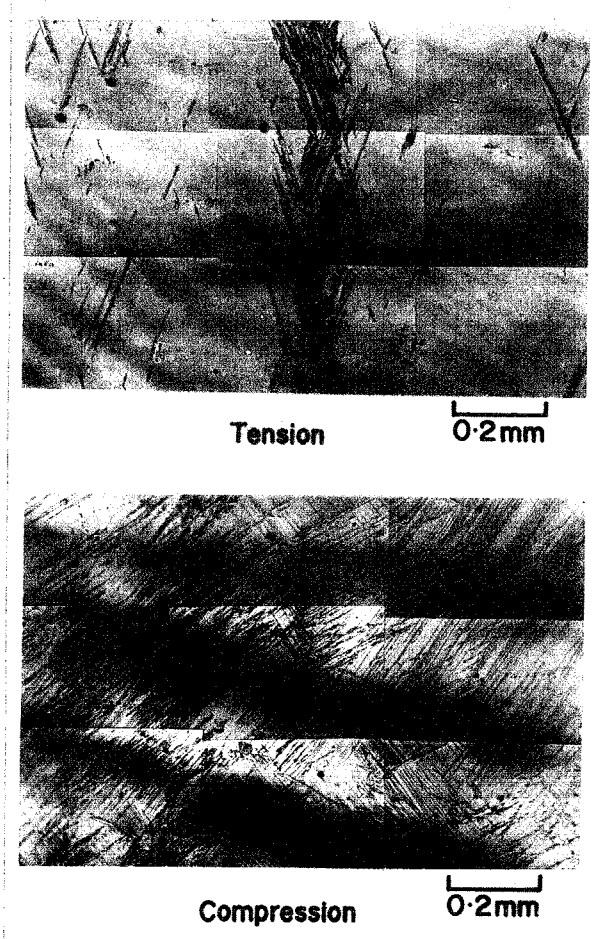

Fig.2.5

Optical micrographs taken from the specimens deformed in tension and in compression in crystal 3. They were deformed by 20 % at 77 K, slightly polished and etched. Horizontal direction corresponds to $[001]_f$.

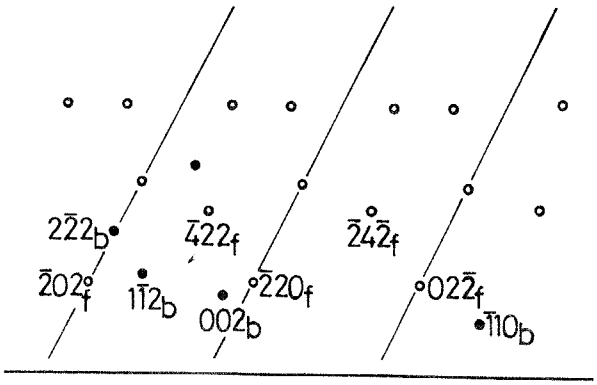

Fig.2.6

X-ray Weissenberg photograph showing the K-S orientation relationship. The specimen was rotated along $[111]_f$.

K-S relationship was conventionally marked. However, this does not essentially change the discussion in the next section.

The determination and notation of twenty-four K-S variants are summarized in Table 2.1. Observed variants in three crystals are as follows:

Crystal 1.

The observed variants in crystal 1 formed under tensile loading at 253 K and 195 K and under compressive loading at 223 K are shown in Table 2.2. Since the geometrical shape of

Table 2.1 Notation of the 24 K-S variants and related shear mechanism by Bogers and Burgers

Variant notation	K-S relation Plane (f′)//(b)	K-S relation Direction [f]//[b]	Twin-related variant	Bogers-Burgers shear mechanism 1st	Bogers-Burgers shear mechanism 2nd
1 - 1	$(\bar{1}1\bar{1})$ (110)	$[10\bar{1}]$ $[\bar{1}1\bar{1}]$	1 - 4	Bα	Cδ
1 - 2		$[0\bar{1}\bar{1}]$ $[\bar{1}11]$	1 - 5	Bα	Dγ
1 - 3		$[\bar{1}\bar{1}0]$ $[\bar{1}1\bar{1}]$	1 - 6	Cα	Dβ
1 - 4		$[\bar{1}01]$ $[\bar{1}11]$	1 - 1	Cα	Bδ
1 - 5		$[011]$ $[\bar{1}1\bar{1}]$	1 - 2	Dα	Bγ
1 - 6		$[110]$ $[\bar{1}11]$	1 - 3	Dα	Cβ
2 - 1	(111) (110)	$[\bar{1}01]$ $[\bar{1}1\bar{1}]$	2 - 4	Cδ	Bα
2 - 2		$[0\bar{1}1]$ $[\bar{1}11]$	2 - 5	Cδ	Aβ
2 - 3		$[1\bar{1}0]$ $[\bar{1}1\bar{1}]$	2 - 6	Bδ	Aγ
2 - 4		$[10\bar{1}]$ $[\bar{1}11]$	2 - 1	Bδ	Cα
2 - 5		$[01\bar{1}]$ $[\bar{1}1\bar{1}]$	2 - 2	Aδ	Cβ
2 - 6		$[\bar{1}10]$ $[\bar{1}11]$	2 - 3	Aδ	Bγ
3 - 1	$(1\bar{1}\bar{1})$ (110)	$[\bar{1}0\bar{1}]$ $[\bar{1}1\bar{1}]$	3 - 4	Aβ	Dγ
3 - 2		$[01\bar{1}]$ $[\bar{1}11]$	3 - 5	Aβ	Cδ
3 - 3		$[110]$ $[\bar{1}1\bar{1}]$	3 - 6	Dβ	Cα
3 - 4		$[101]$ $[\bar{1}11]$	3 - 1	Dβ	Aγ
3 - 5		$[0\bar{1}1]$ $[\bar{1}1\bar{1}]$	3 - 2	Cβ	Aδ
3 - 6		$[\bar{1}\bar{1}0]$ $[\bar{1}11]$	3 - 3	Cβ	Dα
4 - 1	$(\bar{1}11)$ (110)	$[101]$ $[\bar{1}1\bar{1}]$	4 - 4	Dγ	Aβ
4 - 2		$[011]$ $[\bar{1}11]$	4 - 5	Dγ	Bα
4 - 3		$[\bar{1}10]$ $[\bar{1}1\bar{1}]$	4 - 6	Aγ	Bδ
4 - 4		$[\bar{1}0\bar{1}]$ $[\bar{1}11]$	4 - 1	Aγ	Dβ
4 - 5		$[0\bar{1}\bar{1}]$ $[\bar{1}1\bar{1}]$	4 - 2	Bγ	Dα
4 - 6		$[1\bar{1}0]$ $[\bar{1}11]$	4 - 3	Bγ	Aδ

Table 2.2 Interaction energis, U/σ values and observed variants in crystal 1

Variant notation	Crystal 1 with [729]f stress axis: Interaction energy	U/σ value	Observed variants: Tension 253 K	Tension 195 K	Compression 223 K
1 - 1	0.064	-0.075, -0.062			○
1 - 2	0.064	-0.003, 0.052		(1-3′)	
1 - 3	-0.007	0.032, 0.073		○	
1 - 4	-0.007	-0.062, -0.075			○
1 - 5	-0.121	0.052, -0.003			
1 - 6	-0.121	0.073, 0.032	○	○	
2 - 1	0.064	-0.082, -0.067			○
2 - 2	0.064	-0.021, 0.029			
2 - 3	-0.007	0.018, 0.055			
2 - 4	-0.007	-0.067, -0.082	○	○	○
2 - 5	-0.121	0.029, -0.021	○	○	
2 - 6	-0.121	0.055, 0.018			
3 - 1	0.064	-0.027, -0.008			
3 - 2	0.064	0.002, 0.041			○
3 - 3	-0.007	0.051, 0.072			
3 - 4	-0.007	-0.008, -0.027			
3 - 5	-0.121	0.041, 0.002			
3 - 6	-0.121	0.072, 0.051	○	○	
4 - 1	0.064	-0.023, -0.011			
4 - 2	0.064	0.015, 0.052			○
4 - 3	-0.007	0.043, 0.067			
4 - 4	-0.007	-0.011, -0.023			
4 - 5	-0.121	0.052, 0.015	○	○	
4 - 6	-0.121	0.067, 0.043			

the X-ray sample did not permit the quantitative measurement of the distribution of martensite, the circles were put in Table 2.2 if the presence of the variant with the corresponding orientation relationship was detected by the X-ray analysis. One type of the Nishiyama variant, described by

$$(\bar{1}1\bar{1})_f \,//\, (110)_b \ , \ [\bar{2}\bar{1}1]_f \,//\, [\bar{1}10]_b$$

was observed after tensile deformation at 195 K. Since this can be considered as having an intermediate orientation between variants 1-3 and 1-4 of the K-S type, this is denoted as variant 1-3'. Although the specimen deformed in tension at 195 K contained more martensites than that deformed in tension at 253 K, the distribution of the observed variants was essentially identical in both the specimens. Sometimes, twin-related variants were formed; 1-3 (precisely 1-3') ↔ 1-6 in the 195 K specimen, and 1-1 ↔ 1-4 and 2-1 ↔ 2-4 in the 223 K specimen.

The most important fact in Table 2.2 is that, except for the variant 2-4, the variants formed in tension are not observed in compression and vice versa. This demonstrates the strong influence of the sense of the applied stress and the unidirectionality of the deformation associated with the transformation, as previously reported[25].

Crystal 2.

Since the stress-induced martensite studied in the present work is surface martensite, one might speculate that the distribution of martensite is not solely determined by the applied stress direction but also is influenced by the surface orientation. As shown in Fig.2.1, the surface orientation of crystal 2 differs significantly from that of crystal 1, while the stress axes are not markedly different. Thus, in order to examine whether the surface orientation actually affected the distribution of martensites, a specimen of crystal 2 was deformed in tension by 20 % at 77 K. The results of the X-ray analysis are shown in Table 2.3. Besides the variants formed in tension in crystal 1, this specimen contained

Table 2.3 U/σ values and observed variants in crystal 2

Variant notation		Crystal 2 with $[427]_f$ stress axis U/σ value	Observed variants Tension 77 K
1	- 1	-0.074, -0.057	
	- 2	-0.030, 0.030	
	- 3	0.069, 0.091	○
	- 4	-0.057, -0.074	
	- 5	0.030, -0.030	
	- 6	0.091, 0.069	○
2	- 1	-0.087, -0.045	
	- 2	-0.057, 0.000	
	- 3	0.054, 0.066	○
	- 4	-0.045, -0.087	○
	- 5	0.000, -0.057	
	- 6	0.066, 0.054	○
3	- 1	-0.039, 0.005	
	- 2	-0.038, 0.012	○
	- 3	0.083, 0.093	
	- 4	0.005, -0.039	
	- 5	0.012, -0.038	○
	- 6	0.093, 0.083	○
4	- 1	-0.032, 0.004	
	- 2	-0.017, 0.040	
	- 3	0.075, 0.084	
	- 4	0.004, -0.032	
	- 5	0.040, -0.017	○
	- 6	0.084, 0.075	

Table 2.4 Interaction energies, U/σ values and observed variants in crystal 3

Variant notation	Crystal 3 with $[001]_f$ stress axis			
	Interaction energy	U/σ value	Observed variants Tension 77 K	Compression 77 K
1 - 1	0.200	-0.090, -0.009		○
1 - 2	0.200	-0.090, -0.009		
1 - 3	-0.132	0.126, 0.126	○	
1 - 4	-0.132	-0.009, -0.090		
1 - 5	-0.132	-0.009, -0.090	○	
1 - 6	-0.132	0.126, 0.126		
2 - 1	0.200	-0.090, -0.009		
2 - 2	0.200	-0.090, -0.009		○
2 - 3	-0.132	0.126, 0.126	○	
2 - 4	-0.132	-0.009, -0.090		
2 - 5	-0.132	-0.009, -0.090	○	
2 - 6	-0.132	0.126, 0.126	○	
3 - 1	0.200	-0.090, -0.009		○
3 - 2	0.200	-0.090, -0.009		
3 - 3	-0.132	0.126, 0.126	○	
3 - 4	-0.132	-0.009, -0.090		
3 - 5	-0.132	-0.009, -0.090	○	
3 - 6	-0.132	0.126, 0.126		
4 - 1	0.200	-0.090, -0.009		○
4 - 2	0.200	-0.090, -0.009		
4 - 3	-0.132	0.126, 0.126	○	
4 - 4	-0.132	-0.009, -0.090		
4 - 5	-0.132	-0.009, -0.090		
4 - 6	-0.132	0.126, 0.126	○	

some additional variants. A compressive test at 77 K introduced only a few martensite needles so that they were not detected by the Weissenberg technique.

Crystal 3.

The results for crystal 3 which was stressed along $[001]_f$ are listed in Table 2.4. Here again, one can see, as in crystal 1, that the variants formed in tension are not observed in compression and vice versa. However, what is the most significant in crystal 3 is that the compressive loading had stronger tendency to form stress-induced martensites than the tensile loading as was mentioned before and shown in Fig.2.5. Accordingly, one can again find the strong effect of the direction and sense of the applied stress on the formation of stress-induced martensite.

2-4. Discussion

2-4-1. Stress-strain curves and deformation morphology

Contrary to the stainless steel single crystals which show an inverse temperature dependence of yield stress below a critical temperature[26], the yield stress of the single crystals in the present alloy exhibited the normal temperature dependence even when stress-induced martensite was formed during deformation. This change in the temperature dependence is caused by a change

in the relative proportion of deformation occurred by martensitic transformation as compared to slip. In the stainless steel, all deformation takes place by the transformation with the twinning below some definite temperature [3], while, in the present alloy, the deformation occurs by simultaneous slip and transformation as in Fe-30Ni alloy[26]. As concluded by Breedis and Robertson[26], this result appears to indicate that the occurrence of $\gamma \rightarrow \alpha$ transformation is not necessarily responsible for the inverse temperature dependence. In contrast, Bolling and Richman[11,27] and Maki et al[28] reported the presence of the inverse temperature dependence of the yield stress in polycrystalline Fe-Ni(-C) alloys between Ms and M_s^{σ} (the temperature below which the inverse temperature dependence is observed). They attributed the yielding below M_s^{σ} to the $\gamma \rightarrow \alpha$ transformation. However, the observation by Maki et al shows that the larger the grain size, the smaller the inverse temperature dependence and the difference between M_s^{σ} and Ms. In fact, when their observations are extrapolated to the situation of the infinite grain size, M_s^{σ} - Ms goes to zero and the decrease of the yield stress disappears. Thus, it is believed that the present observations as well as those by Breedis and Robertson are not inconsistent with those by Bolling and Richman and Maki et al and that the remarkable decrease of the yield stress of Fe-Ni alloys are only characteristics of the polycrystalline samples.

2-4-2. Crystallography of stress-induced martensite

Throughout the present study, the martensite formed by deformation has been called the stress-induced martensite in order to emphasize that its formation is aided by the applied stress. The fact that the orientation of the martensite variants formed during deformation is critically sensitive to the sense of the applied stress strongly indicates the importance of the applied stress in determining the martensite formation. If the formation of the martensite during the deformation in the present study should be considered as aided by the internal stress field or particular atomic arrangement around defects produced by deformation as discussed by Suzuki et al[29], one should not expect that the distribution of the variants would strongly reflect the sense of the applied stress and of the plastic deformation. For, the dislocations responsible for work hardening are primarily the statistically stored ones[30] in a single phase alloy and the dislocation arrangement should not be sensitive to the sense of the deformation. Furthermore, the absence of the isothermal formation and growth of the martensite in deformed specimens compels one to consider the essential role of the applied stress in martensitic trans-

formation in the present study.

Effect of the applied stress on the martensitic transformation has been examined by several investigators, although it seems that no unified views on the stress effect have been established, as mentioned previously. Therefore, the observed distribution of martensite variants will be examined in several possible manners. This can conventionally be done by using the well-accepted concept of the phenomenological crystallographic theory of martensitic transformation[5,6]. In this theory, total shape deformation of the martensite product T is factorized into lattice deformation B, lattice invariant deformation P and rigid body rotation R. An idea that the applied stress aids the total shape deformation T was first offered by Patel and Cohen[7]. On the other hand, the possibility of the role of the stress on the lattice deformation B was discussed by Olsen and Jesser[12]. Furthermore, Bogers and Burgers [13] explained the experimental results by Bogers[1] using the double shear mechanism which can be understood to consist of the further factorization of the lattice deformation B. Early mechanisms proposed by Kurdjumov and Sachs [31] and Nishiyama[32] also belong to this category. In the following, we would like to discuss the stress effect on the martensitic transformation from several different viewpoints.

i) The factorized component of the lattice deformation B

The dominant shear deformation, which is also common in the three mechanism by Kurdjumov-Sachs, Nishiyama and Bogers-Burgers, occurs on $\{111\}_f\langle 211\rangle_f$. The importance of this shear in the earliest stage of the transformation in Fe-Ni alloy was in fact pointed out by Dash and Brown[33]. Moreover, Higo et al[3] well explained the distribution of stress-induced martensite in an 18-14 stainless steel taking into account the $\{111\}_f\langle 211\rangle_f$ shear systems. Here, the discussion of the $\gamma \rightarrow \alpha$ transformation through the double shear mechanism by Bogers and Burgers will be shown in the following.

Crystallographically possible $\{111\}_f\langle 211\rangle_f$ shear systems are listed in Table 2.5 with the simplified notation by Thompson's tetrahedron together with the Schmid factors for the stress axes in crystals 1, 2 and 3. A shear system with a positive Schmid factor and one with a negative Schmid factor are favored in tension and in compression, respectively.

First, we will discuss the observed distribution of martensite variants in crystal 1. From Tables 2.1, 2.2 and 2.5, one can see that the observed variants 1-6, 3-6 and 4-5 have the shear system $D\alpha(0.491)$ which is the most favorable in tension. The variant 2-5 with the second most favorable shear system $A\delta(0.366)$ was also formed. In the compression specimen, observed

Table 2.5 Schmid factors for the $\{111\}_f\langle 211\rangle_f$ shear systems. Symbols are taken after the Thompson tetrahedron

Shear plane	Shear direction	Schmid factor			Symbol
		Crystal 1	Crystal 2	Crystal 3	
$(\bar{1}1\bar{1})$	$[\bar{1}12]$	-0.305	-0.366	-0.471	Bα
	$[21\bar{1}]$	-0.144	-0.103	0.236	Cα
	$[\bar{1}\bar{2}\bar{1}]$	0.491	0.455	0.236	Dα
(111)	$[11\bar{2}]$	-0.263	-0.337	-0.471	Cδ
	$[\bar{2}11]$	-0.110	0.055	0.236	Bδ
	$[1\bar{2}1]$	0.366	0.307	0.236	Aδ
$(1\bar{1}\bar{1})$	$[1\bar{1}2]$	-0.152	-0.270	-0.471	Aβ
	$[\bar{2}\bar{1}\bar{1}]$	0.170	0.284	0.236	Dβ
	$[12\bar{1}]$	-0.017	-0.021	0.236	Cβ
$(\bar{1}\bar{1}1)$	$[\bar{1}\bar{1}\bar{2}]$	0.033	-0.051	-0.471	Dγ
	$[2\bar{1}1]$	-0.026	0.033	0.236	Aγ
	$[\bar{1}21]$	-0.007	0.018	0.236	Bγ

variants 1-1, 2-1, 3-2 and 4-2 have Bα(-0.305) and/or Cδ(-0.263) which are the first and the second most favorable shear systems in compression.

The existence of twin-related pairs such as 1-3' ↔ 1-6 in tension and 1-1 ↔ 1-4 and 2-1 ↔ 2-4 in compression can be explained in that the formation of one component of the pair was aided by the applied stress and the other component was produced under the influence of the internal stress produced by the former, as discussed previously[3]. The same analysis can also hold in crystal 2 (Table 2.3). Here, observed variants 1-6, 2-6, 3-5, 3-6 and 4-5 have Dα(0.455) or Aδ(0.307) which are the first and the second most favorable shear systems in tension, and the variants 1-3, 2-3 and 3-2 are twin-related with 1-6, 2-6 and 3-5, respectively. Thus, except for the variant 2-4 appeared in tension in both crystals 1 and 2, the Bogers-Burgers mechanism fits very well to explain the formation of the stress-induced variants in the specimens deformed by the asymmetrical stress.

The general trend found in crystals 1 and 2, that the stress-induced martensite is formed in a larger quantity and at a higher temperature in tension than in compression, can be discussed on the same basis as the preceding discussion. For, the largest Schmid factor for the possible shear system of $\{111\}_f\langle 211\rangle_f$ in crystal 1 is 0.491 in tension and 0.305 in compression. This difference accounts for the stronger tendency towards martensite formation under tension in crystal 1. A similar argument can be repeated for crystal 2.

Next, we will discuss the results in crystal 3 with the symmetric $[001]_f$

stress axis. From Tables 2.1, 2.4 and 2.5, one can see that all the observed variants in tension have shear systems with the Schmid factor of 0.236 which is favorable in tension and all the observed variants in compression have shear systems with the Schmid factor of -0.471 which is favorable in compression. Furthermore, the Schmid factor of the favorable systems in compression is twice as large in magnitude as that in tension. This is also in accordance with the experimental observation, Fig.2.5; the compressive loading induces more martensite than the tensile loading. The fact that not all the variants with the same Schmid factor were observed can again be attributed to the unstable direction of the applied stress, i. e., $[001]_f$.

ii) The lattice deformation B

The possibility that the stress mainly affects the Bain deformation in total can be examined by calculating the interaction energy between the stress and the Bain strain[3]. The lattice parameters of the parent phase a_f=3.591 Å, and of the product phase, a_b=2.875 Å [34] and the assumption of the uniformity of elastic constants give the interaction energy, per unit volume of the parent phase, in Tables 2.2 and 2.4 for crystals 1 and 3. Positive and negative values of the interaction energy are favored in compression and in tension, respectively. In the case of crystal 1, the observed variants in tension have the interaction energy of -0.121 which is the most favorable in tension, and two additional variants 1-3' and 2-4. Since the variants 1-3' can be considered as twin-related to 1-6, the formation of 1-3' can be explained rationally. Furthermore, the observed variants in compression, two of which accompany the twin-related variants, have the interaction energy of 0.064, which is the most favorable in compression. The stronger tendency towards martensite formation in tension as compared with that in compression in crystal 1 can again be explained in terms of the interaction energy, for the most favorable interaction energy in tension(-0.121) is almost twice of the most favorable one in compression(0.064).

The same argument entirely holds in crystal 3. That is, all the observed variants in tension have the interaction energy of -0.132, which is favorable in tension, and all the observed variants in compression have the interaction energy of 0.200, which is favorable in compression. Again in this case, compressive stress can introduce more martensites than tensile stress in consistent with the experimental results.

It is not surprising that both the double shear mechanism, such as that proposed by Bogers and Burgers, and the interaction energy between the applied stress and the Bain strain explain the present results equally well, for the

occurrence of the double shear with a little expansion in the parent phase results in the Bain deformation, which can be considered as the initial stage of martensitic transformation.

iii) The shape deformation T

Whether the stress determines the preferential formation of martensite by aiding the shape deformation can be examined by the U/σ value[9]. According to the formulations by Patel and Cohen[7], when a unit volume of the parent phase is transformed into martensite, the work done by the applied stress consists of two terms. That is,

$$U/\sigma = \gamma_o \cos\theta \cdot \cos\lambda + \varepsilon_o \cos^2\theta \qquad (2.1)$$

where U = work done
σ = applied stress
γ_o = total transformation shear strain in the habit plane
ε_o = total transformation strain normal to the habit plane
θ = angle between the habit plane normal and the stress axis
λ = angle between the shear direction and the stress axis.

Goodchild et al[9] and Stone and Thomas[4] used equation (2.1) to examine the crystallographic direction of the applied stress on the martensitic transformation in stainless steels. In the present alloy, it is not certain whether the habit plane does exist, because the morphology of α crystals appears needle-like rather than plate-like. However, for one attempt, the calculation of the U/σ values based on the original Bowles-Mackenzie theory[6] with the $\{101\}_f\langle\bar{1}01\rangle_f$ lattice invariant shear is carried out. The principal distortions of the Bain deformation used in the calculation were $\eta_1=\eta_2=1.1321$ and $\eta_3=0.8005$, resulting in the following habit plane and strains of the total shape deformation.

The habit plane $\{0.1848, 0.7823, 0.5948\}_f$.
The shear strain in the habit plane $\gamma_o=0.224$.
The expansion normal to the habit plane $\varepsilon_o=0.026$.

The calculated results are listed in Tables 2.2, 2.3 and 2.4. Positive and negative values of U/σ are favored in tension and in compression, respectively. In the Bowles-Mackenzie theory, suitable combinations of the compressive axis of the Bain deformation, the lattice invariant shear, and invariant lines and normals lead to the 48 variants, every two of which virtually degenerate to be one K-S variant*. This is the reason why two U/σ values correspond to one variant.

*Strictly speaking, the orientation relationship calculated in the phenomenological theory is a little away from the K-S relationship.

In crystals 1 and 2, the U/σ values show that the variants 1-6, 2-6, 3-6 and 4-6 and their twin-related variants are favored in tension and 1-1, 2-1, 3-1 and 4-1 and their twin-related variants are favored in compression. Although some observed variants may be explained by the U/σ values, the absence of variants 2-6, 4-6(in tension), 3-1, 4-1(in compression) in crystal 1 and 4-6 in crystal 2 cannot be understood. Furthermore, it can be seen that the analysis based on the U/σ values cannot account for the formation of the observed variants 2-4 in tension and 3-2, 4-2 in compression. Such contradictions also appear in discussing the stronger tendency towards martensite formation in tension in crystals 1 and 2, since in crystal 1, the largest value of U/σ is 0.073 in tension while it is 0.082 in compression.

In crystal 3, the similar arguments can also be repeated. Here, as shown in Table 2.4, the observed variants 1-5, 2-5 and 3-5 in tension cannot be understood through the U/σ values. Furthermore, the magnitude of the largest U/σ is 0.090 in compression while it is 0.126 in tension. Thus one cannot help expecting, on the basis of the U/σ, that tension will have a stronger tendency to induce martensite than compression. However, the experimental observation in this respect is just the opposite to the above expectation.

Summarizing the above considerations, the preferential formation of martensite under the stress can be reasonably understood by the postulate that the stress aids the change in lattice. The shape deformation accompanies the additional deformation, slip or twinning, besides the lattice change. It is very unlikely that this additional deformation precedes the lattice deformation. Therefore, it is natural to conclude that the existence of the stress affects the very initial stage of martensitic transformation, where the deformation consists of the lattice change. Unfortunately, the present experimental results cannot discriminate the role played by the Bain strain or by the lattice shears which constitute the Bain strain. However, by taking into account the importance of the cooperative shear movement of atoms as well as the experimental observations such as those by Dash and Brown[33], we would like to emphasize the essential role of the $\{111\}_f\langle 211\rangle_f$ shear system in the initial stage of $\gamma \rightarrow \alpha$ martensitic transformation.

2-5. Conclusion

The morphology and orientation of stress-induced martensite in single crystals of an Fe-23Ni-5Cr alloy were studied. Surface martensite with needle-like surface relief was found in the present study. The distribution

of martensite variants was very sensitive to the direction and sense of the applied stress. Not only the orientation of the stress-induced martensite but also the dependence of the tendency to form martensite on the sense of the applied stress indicate that the applied stress mainly affects the $\{111\}_f$ $<211>_f$ shear systems, operative in the initial stage of the $\gamma \rightarrow \alpha$ lattice change. On the contrary, U/σ values based on the phenomenological theory of martensitic transformation showed no sufficient correlation to the distribution of the orientation of the observed variants and cannot explain the dependence of the tendency towards martensite formation on the sense of the loading. These results imply that the orientation relationship and the distribution of martensite variants under the applied stress are determined in the initial stage of the transformation.

CHAPTER 3

APPLICATION TO MARTENSITIC TRANSFORMATION OF THE ELASTIC PROBLEM IN AN ELLIPSOIDAL INCLUSION WITH PERIODICALLY DISTRIBUTED EIGENSTRAINS

3-1. Motivation and Background

Since Eshelby[18,19,35] gave the attractive solution for the elastic field caused by an ellipsoidal inclusion with a uniformly-distributed eigenstrain (phase transformation strain, plastic strain, thermal strain, etc.) in isotropic media, there have been many works done for the determination of solutions for the elastic fields due to inclusions. Walpole[36], Willis[37] and Kinoshita and Mura[20] extended the problem to the case of inclusions in anisotropic media. The stress field due to linearly-distributed eigenstrain was given by Sendeckyji[38] for isotropic media. Recently, Asaro and Barnett [39] obtained the solution when the eigenstrain is distributed in the form of polynomials with respect to rectangular coordinates.

As implied by Asaro and Barnett[39], an application of the stress field due to a non-uniform eigenstrain in an ellipsoidal inclusion lies in the understanding of martensitic transformation. However, it has been found that martensite plates formed in many martensitic transformations have a structure with alternating twins[40]. Small spherical particles of face-centered cubic Fe in a Cu matrix also transform into martensite with a banded structure[41]. Therefore, the solutions for the elastic field due to eigenstrains distributed in polynomial form throughout an ellipsoidal inclusion are not general enough to solve these problems.

They require the investigation of the elastic field due to a periodic distribution of eigenstrain throughout an inclusion. The alternating twins and banded structure in inclusions can be approximated by periodic distributions of eigenstrains. The elastic solution for such a periodic distribution of eigenstrain throughout an inclusion is also important for more general cases, since any distribution of eigenstrain can be expressed in terms of the Fourier integral or summation of these periodic terms.

Recently, This solution has been offered in a beautiful form by Mura et al[17]. In this work, the solution obtained is used to evaluate the elastic strain energies due to a thin disc of so-called twinned or slipped martensite and to a spherical precipitate with a banded structure induced by martensitic transformation. Previously, these problems of martensitic transformation have been considered by other investigators under some simplification of the dis-

tribution of eigenstrain. For instance, Shibata and Ono[42,43] assumed the distribution to be uniform and Kinsman et al[44] approximated it by a linear function of space coordinates. It will be shown in the present work that significant differences arise when more realistic (periodic) distributions of eigenstrains are considered.

3-2. Fundamental Equation and Flat Ellipsoidal Inclusion

First, the fundamental equation of the displacement component u_i used in a problem of a periodically distributed eigenstrain in an ellipsoidal inclusion, which has been obtained by Mura et al[17], is shown in the following.

We define Ω as an ellipsoidal domain in an infinitely extended medium as

$$\Omega : \quad x_1^2/a_1^2 + x_2^2/a_2^2 + x_3^2/a_3^2 \leq 1 . \tag{3.1}$$

When a distribution of eigenstrain $\varepsilon^*_{nm}(\underset{\sim}{x})$ in a domain Ω can be written in a periodical form as

$$\varepsilon^*_{nm}(\underset{\sim}{x}) = \bar{\varepsilon}^*_{nm} \exp(ic_p x_p/a_p), \quad \text{(sum over p)} \tag{3.2}$$

the displacement component u_i becomes

$$u_i(\underset{\sim}{x}) = \frac{a_1 a_2 a_3}{4\pi} C_{j\ell mn} \bar{\varepsilon}^*_{nm} \int_{S^2} \left\{ (\underset{\sim}{x} \cdot \bar{\underset{\sim}{\xi}}) J_o(c_o R) - i\, c_p a_p \bar{\xi}_p R J_1(c_o R)/c_o \right\}$$

$$\exp\{ i(\underset{\sim}{x} \cdot \bar{\underset{\sim}{\xi}}) c_p a_p \bar{\xi}_p/\zeta^2 \} \frac{\bar{\xi}_\ell N_{ij}(\bar{\underset{\sim}{\xi}})}{\zeta^3 D(\bar{\underset{\sim}{\xi}})} dS(\bar{\underset{\sim}{\xi}}) \tag{3.3}$$

where the reference is to rectangular Cartesian coordinate axes $O(x_i)$ (i=1,2, 3), and the usual summention convention for repeated subscripts applies. In equation (3.3), $C_{j\ell mn}$ are elastic constants, S^2 is on the unit sphere $\bar{\xi}_i \bar{\xi}_i = 1$, J_o and J_1 are Bessel functions of the first kind of the zeroth and first orders, respectively and $N_{ij}(\bar{\underset{\sim}{\xi}})$ and $D(\bar{\underset{\sim}{\xi}})$ are respectively the cofactors and the determinant of the 3×3 matrix with the element $C_{ipjq}\bar{\xi}_p\bar{\xi}_q$ as an (i,j) component.

R, c_o and ζ are defined as

$$\left.\begin{aligned} R &= \{ 1 - (\underset{\sim}{x} \cdot \bar{\underset{\sim}{\xi}})^2/\zeta^2 \}^{1/2} \\ c_o &= \{ c_p c_p - (c_p a_p \bar{\xi}_p/\zeta)^2 \}^{1/2} \\ \zeta &= \{ (a_1\bar{\xi}_1)^2 + (a_2\bar{\xi}_2)^2 + (a_3\bar{\xi}_3)^2 \}^{1/2} \end{aligned}\right\} \tag{3.4}$$

The solution (3.3) is called the fundamental solution. The derivation of (3.3) is shown in Appendix A by quoting the paper by Mura et al[17].

If one of the principal axes, say a_3, becomes zero, (3.3) can be simplified and the total distortion becomes

$$u_{i,k} = C_{j\ell mn}\bar{\varepsilon}^*_{nm}\delta_{\ell 3}\delta_{k3}J_o(c_o)N_{ij}(\underset{\sim}{\bar{\xi}})D^{-1}(\underset{\sim}{\bar{\xi}}) \tag{3.5}$$

where δ_{ij} is the Kronecker's delta and $u_{i,k}$ means the derivative of u_i with respect to x_k. Also for the stress components inside the inclusion:

$$\sigma_{pq} = C_{pqik}\left[C_{j\ell mn}\bar{\varepsilon}^*_{nm}\delta_{\ell 3}\delta_{k3}J_o(c_o)N_{ij}(\underset{\sim}{\bar{\xi}})D^{-1}(\underset{\sim}{\bar{\xi}}) - \bar{\varepsilon}^*_{ki}\exp\{i(c_1x_1/a_1 + c_2x_2/a_2)\}\right] . \tag{3.6}$$

The derivation of (3.5) and (3.6) is shown in Appendix B.

3-3. Application of the Theory to Martensitic Transformations

In this section, we shall evaluate elastic energies due to martensite formation through use of periodically-distributed transformation strains, by using the solutions given in the previous section.

3-3-1. Disc-shaped martensite with alternating twins

In many ferrous alloys, martensites take the form of a thin disc which consists of alternating twins, as shown schematically in Fig.3.1. Each twin can be considered to be formed with the respective transformation strains (eigenstrains). For example, in the case of transformation from F.C.C. to B.C.T.(body-centered tetragonal), the eigenstrains in regions 1 and 2 shown in Fig.3.1 are respectively

$$\overset{1}{\varepsilon}{}^*_{ij} = \begin{pmatrix} \varepsilon_1 & 0 & 0 \\ 0 & \varepsilon_2 & 0 \\ 0 & 0 & \varepsilon_1 \end{pmatrix}, \quad \overset{2}{\varepsilon}{}^*_{ij} = \begin{pmatrix} \varepsilon_2 & 0 & 0 \\ 0 & \varepsilon_1 & 0 \\ 0 & 0 & \varepsilon_1 \end{pmatrix}, \tag{3.7}$$

where the coordinate system is taken along the crystallographic directions of the matrix (x_1, x_2, x_3)-directions in Fig.3.1 (a) and ε_1, ε_2 are given in terms of the lattice constants for the F.C.C. and B.C.T. phases[5], i.e.

$$\varepsilon_1 = \sqrt{2}\ a/a_o - 1, \quad \varepsilon_2 = c/a_o - 1, \tag{3.8}$$

where a_o is the lattice constant for the F.C.C. phase and a, c are the lattice constants for the a- and c-axes of the B.C.T. phase, respectively.

For simplicity, the martensite plate Ω is assumed to have the shape bounded by the surface

$$(x^2 + y^2)/a_1^2 + z^2/a_3^2 = 1, \quad a_3 \ll a_1. \tag{3.9}$$

By taking the x-direction in the direction of the change of the eigenstrain (Fig.3.1 (b)), (3.8) can be written as

$$\varepsilon^*_{ij}(x) = \bar{\varepsilon}^*_{ij}(0) + \sum_{n=1}^{\infty} \bar{\varepsilon}^*_{ij}(n)\cos(2\pi nx/\lambda), \tag{3.10}$$

where

$$\bar{\varepsilon}^*_{ij}(0) = \frac{1}{\lambda}\int_{-\lambda/2}^{\lambda/2} \varepsilon^*_{ij}(x)\, dx$$

$$= f\overset{1}{\varepsilon}{}^*_{ij} + (1 - f)\overset{2}{\varepsilon}{}^*_{ij}, \tag{3.11}$$

$$\bar{\varepsilon}^*_{ij}(n) = \frac{2}{\lambda}\int_{-\lambda/2}^{\lambda/2} \varepsilon^*_{ij}(x)\cos(2\pi nx/\lambda)\, dx, \tag{3.12}$$

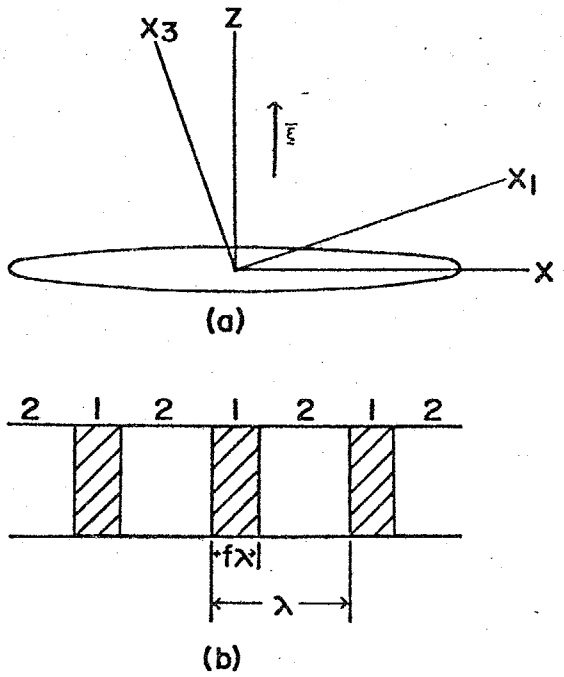

Fig.3.1

Thin-plate martensite, approximated as a flat ellipsoidal inclusion, with alternating twins.

λ being the wavelength describing the periodic distribution of alternating twins and f being the volume fraction of the region 1 ($0 \leq f \leq 1$).

It is tacitly assumed in the phenomenological crystallographic theory of martensitic transformation that the internal stress developed by the eigenstrain, corresponding to the first term in the right side of (3.10), all vanish, if the orientation of the z-axis, $\underset{\sim}{\xi}$ and f take suitable values[45]. In the sequel, it will be shown that even when all the stress components, resulting from the first term in the right side of (3.10) vanish, then there appear non-vanishing stresses due to the second term in the right side of (3.10), resulting in a significant amount of elastic strain energy.

According to the result in Appendix B, the situation when all the stress components resulting from the first term in the right side of (3.10) vanish is achieved by

$$\bar{\varepsilon}^*_{xx}(0) = \bar{\varepsilon}^*_{yy}(0) = \bar{\varepsilon}^*_{xy}(0) = 0, \tag{3.13}$$

where the (x, y, z)-directions are taken in the principal axes directions of the flat ellipsoid. It can be shown that the above condition is attained for four crystallographically equivalent conditions, one of which is described by

$$\bar{\varepsilon}_1 = (1 + \varepsilon_1/\varepsilon_2)^{1/2} , \quad \bar{\varepsilon}_2 = 0 , \quad \bar{\varepsilon}_3 = (-\varepsilon_1/\varepsilon_2)^{1/2} , \tag{3.14}$$

$$f = (1 - \varepsilon_2/\varepsilon_1)^{-1} . \tag{3.15}$$

Since the phenomenological approach employs the finite deformation theory while the present one adopts the infinitesimal theory, (3.14) and (3.15) differ in form from the corresponding expressions obtained from the phenomenological approach. However, because the essential concepts are identical in both approaches, the phenomenological approach leads to the same expression as (3.14) and (3.15) when $(|\varepsilon_1|, |\varepsilon_2|) \ll 1$ (see Wechsler, Lieberman and Read[5], equations (32), (34) and (38)). These correspondence between the present calculation and the phenomenological theory are evident and the process to derive (3.14) and (3.15) can be understood as a 'phenomenological theory based on the infinitesimal deformation approach'.

Of course, as done by Shibata and Ono[42,43] and by Easterling and Thölén [46], the habit plane normal to achieve the minimum elastic energy changes as the value of the aspect ratio $k = a_3/a_1$ changes. However, the choice of any specific non-zero aspect ratio is never justified. Moreover, zero elastic energy is attained only when $k = 0$, obtaining the perfect correspondence to the implication and the calculated consequences in the phenomenological crystallographic theories[5,6].

The above calculation and resultant consequences are due to the assumption that the eigenstrain in the martensite is distributed uniformly. However, in reality, the eigenstrain is distributed periodically as shown in equation (3.10). Now, let us calculate the elastic energy, originating from the presence of the second term in the right side of (3.10), under the condition that (3.14) and (3.15) are satisfied. In this situation, one can take into account the effect of the elastic constants of the martensite usually differing from those of the matrix. Suppose there exists an equivalent inclusion, similar in shape to the martensite plate considered here, with the same elastic constants as the matrix, and which has the eigenstrain

$$\varepsilon^{**}_{ij}(x) = \bar{\varepsilon}^{**}_{ij}(0) + \sum_{n=1}^{\infty} \bar{\varepsilon}^{**}_{ij}(n) \cos(2\pi nx/\lambda) , \tag{3.16}$$

producing distributions of displacement and stress, identical to those produced by the actual martensite plate. The existence of such an equivalent inclusion is assumed if

$$\sigma_{pq} = C_{pqik}(u_{i,k} - \varepsilon^{**}_{ik}) = C^{*}_{pqik}(u_{i,k} - \varepsilon^{*}_{ik}) \tag{3.17}$$

is satisfied, i.e.

$$C_{pqik}\left\{ C_{j\ell mn}\bar{\epsilon}^{**}_{mn}(0)\bar{\xi}_k\bar{\xi}_\ell N_{ij}(\underset{\sim}{\bar{\xi}})D^{-1}(\underset{\sim}{\bar{\xi}}) - \bar{\epsilon}^{**}_{ik}(0)\right\}$$

$$+ C_{pqik}\left\{\sum_{n=1}^{\infty} C_{j\ell mn}\bar{\epsilon}^{**}_{mn}(n)\bar{\xi}_k\bar{\xi}_\ell J_o\left(\frac{2\pi a}{\lambda}n\right)N_{ij}(\underset{\sim}{\bar{\xi}})D^{-1}(\underset{\sim}{\bar{\xi}})\right.$$

$$\left. - \sum_{n=1}^{\infty} \bar{\epsilon}^{**}_{ik}(n)\cos\frac{2\pi n}{\lambda}x\right\}$$

$$= C^*_{pqik}\left\{ C_{j\ell mn}\bar{\epsilon}^{**}_{mn}(0)\bar{\xi}_k\bar{\xi}_\ell N_{ij}(\underset{\sim}{\bar{\xi}})D^{-1}(\underset{\sim}{\bar{\xi}}) - \bar{\epsilon}^{*}_{ik}(0)\right\}$$

$$+ C^*_{pqik}\left\{\sum_{n=1}^{\infty} C_{j\ell mn}\bar{\epsilon}^{**}_{mn}(n)\bar{\xi}_k\bar{\xi}_\ell J_o\left(\frac{2\pi a}{\lambda}n\right)N_{ij}(\underset{\sim}{\bar{\xi}})D^{-1}(\underset{\sim}{\bar{\xi}})\right.$$

$$\left. - \sum_{n=1}^{\infty} \bar{\epsilon}^{*}_{ik}(n)\cos\frac{2\pi n}{\lambda}x\right\}, \qquad (3.18)$$

where C_{pqik}, C^*_{pqik} are the elastic constants of the matrix and the martensite, respectively. Suppose that we take

$$\bar{\epsilon}^{**}_{ik}(0) = \bar{\epsilon}^{*}_{ik}(0) , \qquad (3.19)$$

and, then, the first terms in the left and right sides of (3.18) disappear, since we have chosen $\bar{\epsilon}^{*}_{ik}(0)$ so that all the stresses produced by it vanish. Thus, (3.18) reduces to

$$C_{pqik}\left\{\sum_{n=1}^{\infty} C_{j\ell mn}\bar{\epsilon}^{**}_{mn}(n)\bar{\xi}_k\bar{\xi}_\ell J_o\left(\frac{2\pi a}{\lambda}n\right)N_{ij}(\underset{\sim}{\bar{\xi}})D^{-1}(\underset{\sim}{\bar{\xi}}) - \sum_{n=1}^{\infty} \bar{\epsilon}^{**}_{ik}(n)\cos\frac{2\pi n}{\lambda}x\right\}$$

$$= C^*_{pqik}\left\{\sum_{n=1}^{\infty} C_{j\ell mn}\bar{\epsilon}^{**}_{mn}(n)\bar{\xi}_k\bar{\xi}_\ell J_o\left(\frac{2\pi a}{\lambda}n\right)N_{ij}(\underset{\sim}{\bar{\xi}})D^{-1}(\underset{\sim}{\bar{\xi}})\right.$$

$$\left. - \sum_{n=1}^{\infty} \bar{\epsilon}^{*}_{ik}(n)\cos\frac{2\pi n}{\lambda}x\right\} . \qquad (3.20)$$

Electron microscopic observation has shown that $a \approx 10$ μm and $\lambda \approx 100$ Å[40]. Thus, the requirement for the existence of the equivalent inclusion is given by the condition

$$- C_{pqik} \sum_{n=1}^{\infty} \bar{\varepsilon}^{**}_{ik}(n) \cos \frac{2\pi n}{\lambda} x$$

$$= - C^{*}_{pqik} \sum_{n=1}^{\infty} \bar{\varepsilon}^{*}_{ik}(n) \cos \frac{2\pi n}{\lambda} x \ . \qquad (3.21)$$

Of course, (3.21) is satisfied if $C_{pqik}\bar{\varepsilon}^{**}_{ik}(n) = C^{*}_{pqik}\bar{\varepsilon}^{*}_{ik}(n)$. From (3.18), (3.21) and (3.10), the stress σ_{pq} through the martensite plate is written as

$$\sigma_{pq}(x) = - C^{*}_{pqik} \{ \varepsilon^{*}_{ik}(x) - \bar{\varepsilon}^{*}_{ik}(0) \} \ . \qquad (3.22)$$

The elastic energy $E_{e\ell}$ is calculated from the expression[35]

$$E_{e\ell} = - \frac{1}{2} \int_{\Omega} \sigma_{pq} \varepsilon^{*}_{pq} \, dv \ , \qquad (3.23)$$

where dv is the volume element. Thus, from (3.23), (3.22) and (3.7), the elastic energy E_o due to unit volume of martensite plate is computed as

$$E_o = E_{e\ell}/\Omega = f(1 - f)(C^{*}_{11} - C^{*}_{12})(\varepsilon_1 - \varepsilon_2)^2 \ , \qquad (3.24)$$

where f is given by (3.15) and $C^{*}_{11} = C^{*}_{1111}$, $C^{*}_{12} = C^{*}_{1122}$. By using numerical values adequate for an Fe-22%Ni-0.8%C alloy (ε_1 =0.1201 and ε_2 =-0.1723)[5] with $C^{*}_{11} = 2.37 \times 10^{11}$ and $C^{*}_{12} = 1.41 \times 10^{11}$ N/m^2, one obtains from (3.24) the elastic energy of the martensite as 1.4×10^{4} J/mol. The fact that this value is considerably large is significant in three respects as follows. (i) The phenomenological theory of martensitic transformation takes account of only the first term in the right side of (3.10). The condition that the elastic energy vanishes under this situation results in the significant amount of the elastic energy, if one takes into account the second term in the right side of (3.10). It seems that the postulate and the resultant indication in the phenomenological theory require refinement and modification. (ii) F.C.C. → B.C.T.(or B.C.C.) martensitic transformation of ferrous alloys occurs in a considerably supercooled state. This is attributed partly to the elastic energy associated with martensite formation (Note that the above supposition is in contradictory to the tacitly assumed postulate of the phenomenological theory.) In steels, it is said that the martensitic transformation occurs only when the supercooled state in which the free energy difference between the γ-phase and martensite becomes as much as 1.3×10^{3} J/mol[47]. Thus, the order of magnitude of the elastic energy calculated from (3.24) is sufficient

enough to explain the necessity of the supercooling for the transformation to occur. (iii) It is difficult to consider some relaxation mechanisms, such as those envisaged by Kajiwara and Owen[48], which occur inside a martensite plate and for which the elastic energy is reduced, because the alternating twin structure itself has been adopted as a relaxation mechanism. In order to reduce the elastic energy, It seems that one has to seek relaxation processes, involving dislocation motion, which take place outside the martensite.

The experimental observations which have established the existence of twinned martensite plates might nullify the conclusion reached above. However, it should be pointed out that the twinned martensite has been observed only in a thin film or on a surface. It has never been established that inside a bulk crystal martensite plates are also twinned and have a form, consistent with the prediction by the phenomenological theory. The evaluation of the elastic energy, conducted above, assumes the infinitely extended material, corresponding to the situation where a martensite plate is actually present in a bulk crystal. In other words, the elastic state has been relaxed only by removing the constriction by the matrix, even when one claims that the twinned martensite plate has actually been observed.

3-3-2. Disc-shaped martensite with slip

Martensite plates with slip as a lattice invariant shear have also been observed in many alloys. In this case, one can treat the elastic calculation in a similar manner as in the previous section.

For example, in case of the transformation from F.C.C. to B.C.T., the transformation strain in the martensite plate approximated as the flat ellipsoidal inclusion Ω described by (3.9) becomes

$$\varepsilon_{ij}^{T} = \begin{pmatrix} \varepsilon_2 & 0 & 0 \\ 0 & \varepsilon_1 & 0 \\ 0 & 0 & \varepsilon_1 \end{pmatrix} . \qquad (3.25)$$

Shibata and Ono in their first paper[42] and Clarke[49] considered, in essence, only the equation (3.25) as the eigenstrain involved in the transformation. However, one cannot obtain the situation of zero elastic energy by taking only ε_{ij}^{T} into account. On the viewpoint of the phenomenological theory, this corresponds to the fact that the situation of the existence of an undistorted plane cannot be attained by the pure Bain deformation. Thus, one must consider an additional plastic deformation either by slip or by twinning —

lattice invariant deformation — in the martensite to find the zero elastic energy state. In order to treat the case which corresponds to the situation calculated and predicted by the phenomenological theory, the assumption that the lattice invariant shear occurs on $(110)_f[1\bar{1}0]_f$ is adopted in the calculation. Considering that the slip in a real crystal must be induced by the motion of perfect dislocations, the Burgers vector of which is determined crystallographically. This physically means that the slip in the martensite cannot occur uniformly. In other words, a slipped martensite can be understood consisting of regular arrangements of the alternating slipped and unslipped regions. In the case of a twinned martensite, this fact corresponds to the existence of alternating two kinds of twinned regions as previously discussed.

Let $\varepsilon^P_{ij}(x)$ be the eigenstrain caused by the slip deformation which differs from place to place periodically in the martensite. One can write the total eigenstrain, due to the lattice change and slip, as

$$\begin{aligned}\overset{*}{\varepsilon}_{ij}(x) &= \varepsilon^T_{ij} + \varepsilon^P_{ij}(x) \\ &= \varepsilon^T_{ij} + \bar{\varepsilon}^P_{ij}(0) + \sum_{n=1}^{\infty} \bar{\varepsilon}^P_{ij}(n) \cos\frac{2\pi}{\lambda} nx \ , \end{aligned} \tag{3.26}$$

where

$$\begin{aligned}\bar{\varepsilon}^P_{ij}(0) &= \frac{1}{\lambda}\int_{-\lambda/2}^{\lambda/2} \varepsilon^P_{ij}(x)\, dx \ , \\ \bar{\varepsilon}^P_{ij}(n) &= \frac{2}{\lambda}\int_{-\lambda/2}^{\lambda/2} \varepsilon^P_{ij}(x) \cos\frac{2\pi}{\lambda} nx\, dx \ . \end{aligned} \tag{3.27}$$

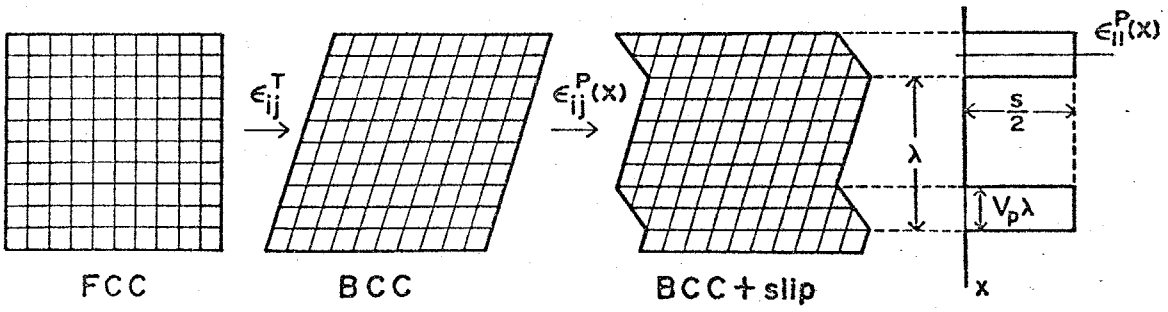

Fig. 3.2

Schematic representation showing the periodic distribution of the slip deformation in a martensite. Note that the eigenstrain by slip is introduced periodically.

Here, we have assumed that the slip occurs with the periodicity of λ. The assumption that the ε^{P}_{ij} is a function of x is justified, since we are considering the plate martensite.

Adopting V_p ($0 \leq V_p \leq 1$) as the fraction of the slipped region in the martensite and s as the amount of slip to be determined crystallographically, the second term in (3.26) can be written as

$$\bar{\varepsilon}^{P}_{ij}(0) = \begin{pmatrix} V_p s/2 & 0 & 0 \\ 0 & -V_p s/2 & 0 \\ 0 & 0 & 0 \end{pmatrix} . \tag{3.28}$$

The situation of (3.26), (3.27), (3.28) is schematically shown in Fig.3.2. (3.28) corresponds to the average amount of the lattice invariant shear, and if by considering only $\varepsilon^{T}_{ij} + \bar{\varepsilon}^{P}_{ij}(0)$ as eigenstrains, the elastic energy becomes zero when the unit vector $\underset{\sim}{\bar{\xi}}$, parallel to the z-axis (habit plane normal) and $V_p s$ take the following values;

$$\left.\begin{aligned} \underset{\sim}{\bar{\xi}} &= \left(\left(1 + \varepsilon_1/\varepsilon_2\right)^{1/2},\ 0,\ \left(-\varepsilon_1/\varepsilon_2\right)^{1/2} \right), \\ V_p s &= 2\varepsilon_1 . \end{aligned}\right\} \tag{3.29}$$

As mentioned before, when $|\varepsilon_1|$ and $|\varepsilon_2|$ are small, the corresponding expressions derived from the phenomenological calculation become identical to (3.29).

Our task is to evaluate the elastic energy due to the third term in (3.26) which was overlooked in the past, under the condition that (3.29) is fulfilled. By taking the same procedure as that adopted in the previous section, the elastic energy per unit volume of martensite in the situation described by (3.26) and (3.29) is calculated as

$$E_o = V_p(1 - V_p)(C^*_{11} - C^*_{12})(s/2)^2 , \tag{3.30}$$

where C^*_{11} and C^*_{12} are the elastic constants of the martensite. In the slipped region, we assume p (p = 1, 2, 3,...) dislocations have passed on every slip plane. From the crystallographic consideration, s is evaluated as

$$s = \frac{(1 + \varepsilon_1)^2 + (1 + \varepsilon_2)^2}{(1 + \varepsilon_1)(1 + \varepsilon_2)}\, p , \tag{3.31}$$

where the slip along the $[1\bar{1}\bar{1}]_b$ on the $(211)_b$ is considered, corresponding to the $(110)_f[1\bar{1}0]_f$ system. With (3.8), if a and c are equal (B.C.C. lattice), (3.31) can be simplified and is rationally written as

$$s = \frac{3\sqrt{2}}{2} p \ . \qquad (3.32)$$

This can be considered as the consequence that p dislocations with the Burgers vector $\underset{\sim}{b} = (a/2)[1\bar{1}\bar{1}]_b$ have passed on every $(211)_b$ plane. It should be noted that if one pursues the infinitesimal deformation approach in expressing s, (3.31) can be simplified and is rationally written as

$$s = 2p \ . \qquad (3.33)$$

In fact, (3.32) and (3.33) differ only by 6 %.

The elastic energy, given by (3.30), is shown to take a minimum when p = 1, that is,

$$V_p = \varepsilon_1 \ . \qquad (3.34)$$

Using adequate values of ε_1 and ε_2 for an Fe-31Ni alloy ($\varepsilon_1 = 0.1321$ and $\varepsilon_2 = -0.1995$[45]) with $C_{11}^* = 2.37$ and $C_{12}^* = 1.41 \times 10^{11}$ N/m^2, one obtains the elastic energy of 7.8×10^4 J/mol of the martensite from (3.30).

What must be emphasized here is that the significant contribution of the periodically distributed lattice invariant deformation, which has been, until now, overlooked, should be considered in the energetics involving the martensitic transformation. The discussions on this matter in the present study are identical to those presented in the last paragraph of 3-3-1.

Here, we would like to comment on some recent developments in the phenomenologocal theory. In order to explain the $\{225\}_f$ habit plane found in the stainless steel or the complicated internal traces in the martensite plate, several efforts have recently been made by introducing the so-called dilatation parameter[16] or multiple lattice invariant shears[14,15] to the original phenomenological theory. However, the dilatation parameter which is translated into Japanese, "整合パラメーター", sometimes cheating one by a vaguely defined word, "整合", and is adjusted to match the calculation with the observation is a quantity which cannot find itself in physics in the deformation associated with the martensitic transformation. It is an arbitrary quantity to please those who use it. The introduction of more than one lattice invariant shear also enables one to select arbitrary parameters. To show this, an example of the calculation will be given in Appendix C which proves that any plane can be a habit plane, in the context of the phenomenological theory, if at least three independent shear systems are assumed to operate in the lattice invariant deformation. In short, the introduction of arbitrary parameters spoils the beauty possessed by the original phenomenological theory when

it was born.

3-3-3. Spherical precipitate undergoing martensitic transformation

A spherical iron precipitate, which is formed in a copper matrix and is F.C.C. before martensitic transformation, becomes B.C.C. with the banded structure of alternating twins after transformation. The elastic energy of an iron particle with the banded structure has recently been evaluated by Kinsman et al[44] with an unrealistic approximation based on a simplified model. The physical situation envisaged by them is that a spherical region undergoes martensitic transformation, the upper and the lower halves shearing in anti-parallel directions, as shown schematically in Fig.3.3 (a). Thus, the surface and the eigenstrain of the transformed particle Ω should be respectively

$$(x_1^2 + x_2^2 + x_3^2)/a^2 = 1 \ , \tag{3.35}$$

$$\varepsilon_{31}^*(\underset{\sim}{x}) = \pm \frac{1}{2} S \ , \quad x_3 \gtrless 0 \quad \text{in } \Omega \ , \tag{3.36}$$

where a is the radius of the spherical particle and S is a constant to be determined by crystallographic information. However, Kinsman et al[14] approximated the above situation with the eigenstrain

$$\varepsilon_{31}^*(\underset{\sim}{x}) = t x_3/a \quad \text{in } \Omega \ , \tag{3.37}$$

with t = S, in order to utilize Asaro and Barnett's work[39]. In the sequel,

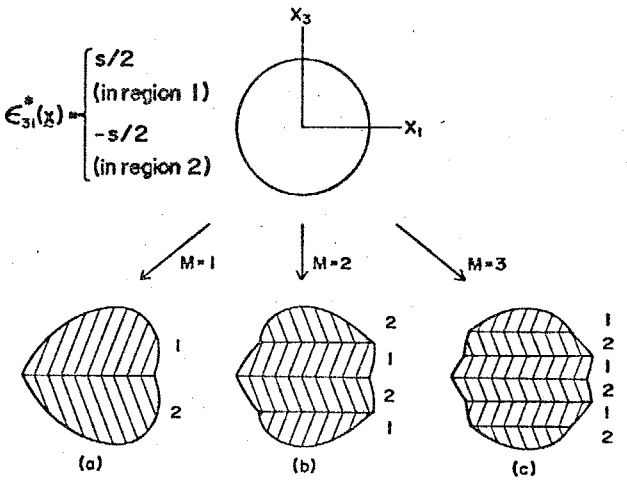

Fig.3.3

Spherical precipitate undergoing martensitic transformation. When matrix constraint is absent, the spherical particle changes its shape successively to (a),(b) and (c) to form twinned martensite.

the elastic energy assicoated with the situation described by (3.35) and (3.36) will be calculated.

The Fourier series expressed for the eigenstrain (3.36) is

$$\varepsilon^{*}_{31}(\underset{\sim}{x}) = (2S/\pi)\sum_{n=1}^{\infty}(2n-1)^{-1}\sin((2n-1)\pi x_3/a) \ . \tag{3.38}$$

For simplicity, the spherical precipitate and the matrix will be assumed to have the same isotropic elastic constants. From (3.3) and (3.38), the only non-vanishing stress component σ_{31} pertinent to the strain energy evaluation becomes

$$\sigma_{31}(\underset{\sim}{x}) = \sum_{n=1}^{\infty}\bar{\sigma}_{31}(\underset{\sim}{x}, n) \tag{3.39}$$

with

$$\begin{aligned}\bar{\sigma}_{31}(\underset{\sim}{x},n) = \frac{\mu S a^3}{\pi C_3}\int_{S^2}\Big[& J_o(C_oR)\sin\left\{(\underset{\sim}{x}\cdot\bar{\underset{\sim}{\xi}})C_3\bar{\xi}_3/a\right\} \\ & + 2J_o(C_oR)C_3\bar{\xi}_3(\underset{\sim}{x}\cdot\bar{\underset{\sim}{\xi}})\cos\left\{(\underset{\sim}{x}\cdot\bar{\underset{\sim}{\xi}})C_3\bar{\xi}_3/a\right\}/a \\ & + J_1(C_oR)\left\{(\underset{\sim}{x}\cdot\bar{\underset{\sim}{\xi}})^2 C_o/(a^2R) + C_3^2\bar{\xi}_3^2 R/C_o\right\}\sin\left\{(\underset{\sim}{x}\cdot\bar{\underset{\sim}{\xi}})C_3\bar{\xi}_3/a\right\}\Big] \\ & \times(\bar{\xi}_1^2+\bar{\xi}_3^2-3\bar{\xi}_1^2\bar{\xi}_3^2)dS(\bar{\underset{\sim}{\xi}}) - (4\mu S/C_3)\sin(C_3x_3/a) \ . \end{aligned} \tag{3.40}$$

where $C_3 = (2n-1)\pi$, μ is the shear modulus, and Poisson's ratio is taken to be 1/3. Since the analytical integration involved in (3.40) is difficult, the stress and the elastic energy to be determined from (3.23) have been evaluated numerically on a computer. The procedure employed in the numerical computation is as follows. (i) The Fourier series in (3.38) and (3.39) are truncated at n = 16; it seems (empirically) that this truncation does not introduce any significant error, since the calculated elastic energy with the truncation at n = 20 differs from that at n = 16 only by 0.5 %. (ii) Since

$$\sigma_{31}(x_1,x_2,x_3) = \sigma_{31}(-x_1,x_2,x_3) = \sigma_{31}(x_1,-x_2,x_3) = \sigma_{31}(x_1,x_2,-x_3) \ ,$$

it is sufficient to consider a one-eighth part of Ω, this being divided into 114 identical volume elements. By means of the above procedure, it has been found that the situation corresponding to (3.35) and (3.36) gives the elastic energy as

$$E_{el} = 0.365\mu S^2\Omega/2 \tag{3.41}$$

The value (3.41) is a little larger than Kinsman et al's value[44] based on the approximate distribution of eigenstrains. Similar calculations have been performed for the cases

$$\varepsilon^*_{31}(\underset{\sim}{x}) = \begin{cases} \frac{1}{2} S , & 2Na/M < x_3 < (2N+1)a/M, \\ -\frac{1}{2} S , & (2N+1)a/M < x_3 < (2N+2)a/M, \end{cases} \quad \text{in } \Omega , \qquad (3.42)$$

with M = 2, 3, 4 (see Fig.3.3), (the case M = 1 corresponds to (3.36)). In (3.42), N takes integer values. The calculated elastic energies are plotted against M in Fig.3.4, which also includes results for the case M = 0, corresponding to uniform shear and Kinsman et al's value for the case M = 1. It can be seen that as M increases, then the elastic energy decreases. Thus, as far as the elastic energy is concerned, the alternating twin structure with the shorter interval is favored. This conclusion matches with intuition, based on an examination of Fig.3.3; as the interval between the alternating twins decreases, the change in shape of the particle caused by the transformation becomes smaller as a whole.

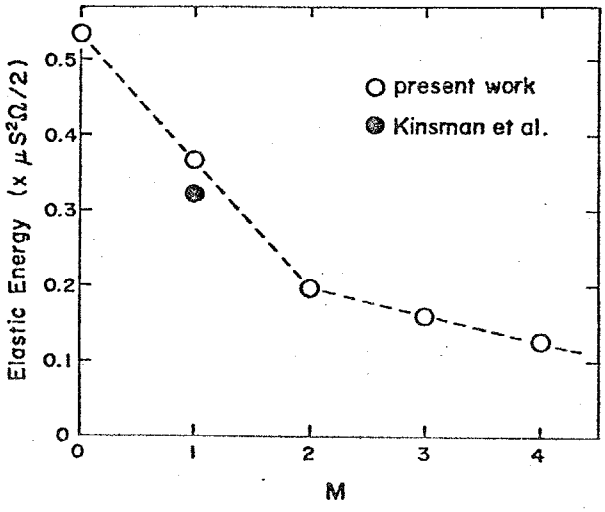

Fig.3.4
Elastic energy of a martensite particle with M pairs of twins.

It is to be noted that in order to explain the observed value of M in a real Cu-Fe alloy, not only the elastic energy calculated above but also the specific twin-interface energy must be considered. This will be discussed in Chapter 4.

3-4. Conclusion

The solution for the elastic field caused by a periodic distribution of eigenstrains in an ellipsoidal inclusion was applied to the disc-shaped and spherical martensites to estimate the elastic energy associated with the transformations.

The applications illustrate the importance of periodically-varying eigenstrains for the contribution to elastic energies. If uniform average eigenstrains are used for the disc-shaped martensite, then the minimum elastic energy becomes zero, resulting in the perfect correspondence to what the phenomenological crystallographic theory seeks. However, if one duly considers the periodic distribution of eigenstrains in the disc-shaped martensite, a

large amount of the elastic energy does exist which never becomes zero. This is an attractive result indicating that the implication of the phenomenological theory must be re-examined.

The calculation for elastic energy due to the spherical martensite with alternating twins shows that the elastic energy per unit volume of the martensite is a decreasing function of the number of twin pairs.

CHAPTER 4

STRESS-INDUCED MARTENSITE OF SPHERICAL IRON PARTICLES IN A Cu-Fe ALLOY

4-1. Motivation of the Study

In Chapter 2, it has been concluded that applied stress plays a role in the $\gamma \rightarrow \alpha$ martensitic transformation by aiding the shear deformation associated with the lattice change rather than the total shape change, which is one of the quantities calculated by the phenomenological crystallographic theory. It is well known that γ-iron precipitates formed in Cu-Fe alloys and surrounded by the copper matrix undergo a $\gamma \rightarrow \alpha$ martensitic transformation when external stress is applied[50]. However, the shape of this α-iron martensite is spherical and is very different from that of other martensites in ferrous alloys. Such a spherical shape is outside of the calculation in the phenomenological theory in its present form. However, it certainly appears that the total shape deformation varies when the form of martensite changes considerably. Consequently, if applied stress plays a dominant role on the preferential formation of martensite by aiding the shape deformation, one can expect that the orientation of martensite preferentially formed under stress varies with the shape of martensite. On the other hand, if the preferential formation of martensite is understood through the shear deformation in the lattice change, the similar variants of martensite can be expected to be formed regardless of the shape of martensite. With this in mind, the present study has examined $\gamma \rightarrow \alpha$ martensitic transformation of the spherical iron particles in a Cu-1.06Fe alloy single crystal by examining the orientation of the preferentially formed martensites with respect to the stress direction.

The α-iron martensite in a copper matrix possesses the banded structure which was first considered as alternative layers of α- and γ-iron discs[41]. Recently, Kinsman et al have shown that the bands consist of two types of twinned variants with nearly the Kurdjumov-Sachs orientation relationship to the parent copper matrix[44]. In a recent paper[17], the solution of the elastic state of an ellipsoidal inclusion with a periodic distribution of eigenstrain (transformation strain) has been presented, as edited in Appendix A, and its applicability to the evaluation of the elastic energy due to a martensite with alternating twins has been shown in Chapter 3. It has been indicated that the elastic energy caused by a spherical martensite with alternating twins decreases as the number of the twin bands increases. On the other hand, the alternating twins induce the additional twin-interface energy which

is an increasing function of the number of bands. The elastic energy and the twin-interface energy have different dependences on the particle size. Thus, one can expect that the number of the twin bands depends on the particle size. This chapter will also examine this possibility experimentally. Further, we will try to obtain an information on the specific twin-interface energy in B.C.C. iron by extending and conducting the previous calculation in 3-3-3 with some constants relevant to the present study.

4-2. Experimental Procedure

Single crystals of a Cu-1.06wt%Fe alloy were grown by the Bridgman method. After determining the orientation of the crystal by the back-Laue technique, tensile($3 \times 3 \times 40$ mm) and compressive ($3 \times 3 \times 6$ mm) specimens were spark-cut from the as-grown single crystals. These specimens were then solution-treated at 1233 K in vacuum for 6 hours and water quenched. Various sizes of γ-iron particles were obtained by aging the specimens at 973 K in vacuum for from 6 hours to 7 days. After these sequences, γ-iron particles with about 200 $\sim$ 2000 Å in diameters could be obtained. The γ-iron particles did not transform to equilibrium α-iron after either 7 day aging or simple cooing to 77 K, in agreement with the previous study[50].

Uniaxial tensile and compressive stresses were applied along approximately $[416]_f$ direction at 77 K using an Instron-type testing machine to induce $\gamma \rightarrow \alpha$ martensitic transformation inside the iron particles. These single crystals were sliced parallel to several different $\{111\}_f$ planes by a spark-cutter. Thin foils were prepared from the discs by the jet polishing technique using a chromic-acetic acid solution. The internal structure and the distribution of martensite variants in the iron particles were observed on an electron microscope (Hitachi H-700), equipped with a 60 degrees goniometer, under an acceleration voltage of 200 kV.

4-3. Experimental Results

4-3-1. Martensite variants after deformation

As the $\gamma \rightarrow \alpha$ martensitic transformation in the iron particles in this alloy begins in the very early stage of the deformation, specimens were deformed as much as 5 % tensile (compressive) strain at 77 K. In practice, magnetic mesurement after this deformation indicated the occurrence of the $\gamma \rightarrow \alpha$ transformation in the iron precipitates. The characteristics of the

deformation behaviour shown in Fig. 4.1 were similar to those in the previous works[51,52], i.e., the yield stress was given by Orowan's relation and the initial work-hardening rate was small. From electron microscopic observation of the specimens, it was found that the orientation relationship between the α-iron particles and the copper matrix was approximately 2° away from the K-S type. This relationship had also been observed by Easterling and Weatherly[53]. Very often, twin-related diffraction spots from the α-iron particles were observed.

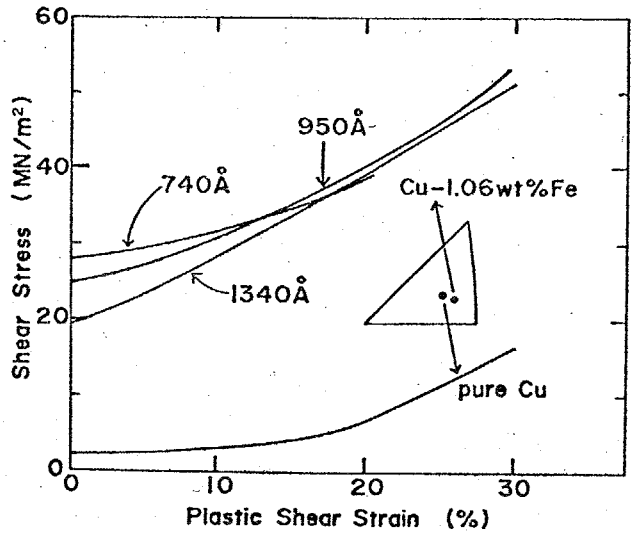

Fig.4.1

Stress-strain curves of Cu-1.06%Fe alloy single crystals deformed at 77 K in tension. For comparison, a curve of pure Cu single crystal was also drawn. Standard triangle shows the tensile directions.

Figure 4.2 shows the typical appearances of the α-iron particles taken from the primary $(1\bar{1}1)_f$ plane after the compressive deformation; (a) is a bright field image, (b) and (c) are dark field images taken by using the two kinds of α-iron spots which are twin-related to each other. From these photographs, one can see that an α-iron particle consists of alternating bands of twin-related martensites. In particles with 200 ∿ 1500 Å in diameters, such banded appearances could in most cases be resolved from some definite directions when a thin foil specimen was rotated in the electron microscope. Another feature to note in Fig.4.2 is that the bands in most particles are equi-directionally aligned in the same direction. This was common among all the area examined and shows the strong influence of the applied stress on the martensitic transformation, i.e., applied stress aids the preferential formation of the specific martensite variants among the crystallographically equivalent ones. These bands are parallel to the $\{211\}_b$ twinning plane which are approximately parallel to $\{110\}_f$ matrix plane. The particles larger than ∿1500 Å showed rather complicated internal structures as had been reported by Kinsman et al[44]. The dark field analysis of these large particles indicated that they consisted of more than two variants of martensite. From this reason, the deformed specimens, which had been aged for 2 days and in which the particles had an average diameter of 950 Å and showed a simple structure such as shown in Fig.4.2 were mainly observed for the crystallographic analysis.

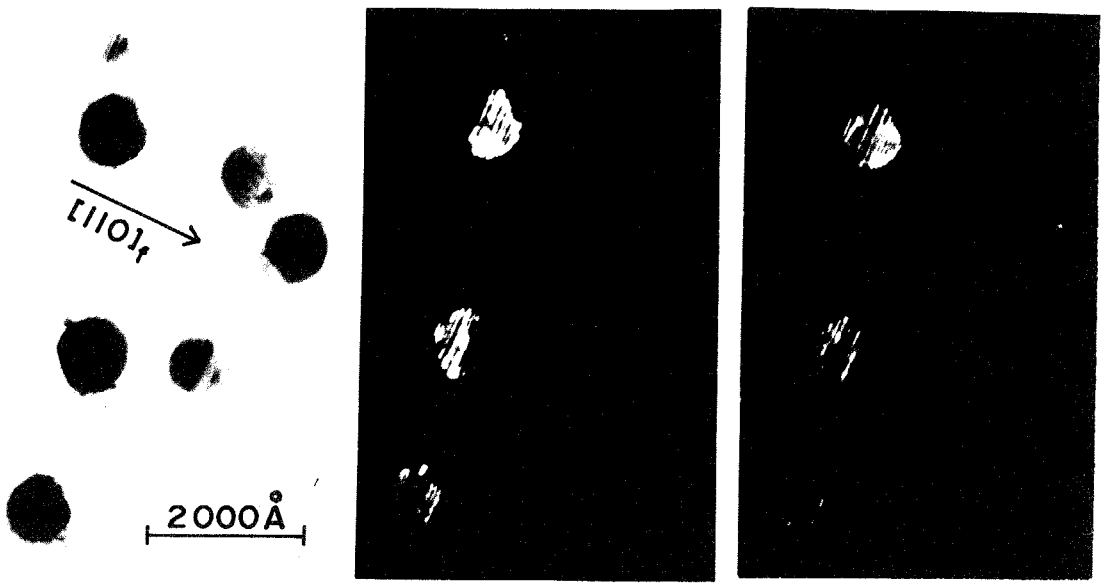

(a) (b) (c)

Fig.4.2

Electron micrographs of α-Fe particles. The specimen was deformed by 5 % in compression at 77 K after 2 day aging at 973 K. Matrix plane is parallel to the primary $(1\bar{1}1)_f$ plane. (a) is a bright field image and (b) and (c) are dark field images using two kinds of the α-Fe spots which are twin-related to each other.

In order to examine the effect of the sense of the loading on the transformation, the orientations of the preferentially formed martensite variants were determined by the dark field analysis, using the electron beam normal to $\{111\}_f$ planes. The example of this analysis is given in Fig.4.3. The photographs were taken from the $(1\bar{1}1)_f$ plane of the specimen which had been deformed under tensile stress after 2 day aging. More than 400 particles were statistically examined and the final results of the distribution of the variants both in tension and in compression are listed in Table 4.1†. As can be seen easily, there is a strong dependence of the distribution of the martensite variants on the sense of the loading. This will be discussed later.

4-3-2. Particle size dependence of the banded structure

As stated before, the iron particles with about 200 ∿ 2000 Å in diameter were obtained by varying the aging time. The banded structure of alternating

† Here, we have assumed that the martensite has the K-S orientation relationship to the parent phase. That is, the nearest K-S variants were conventionally marked.

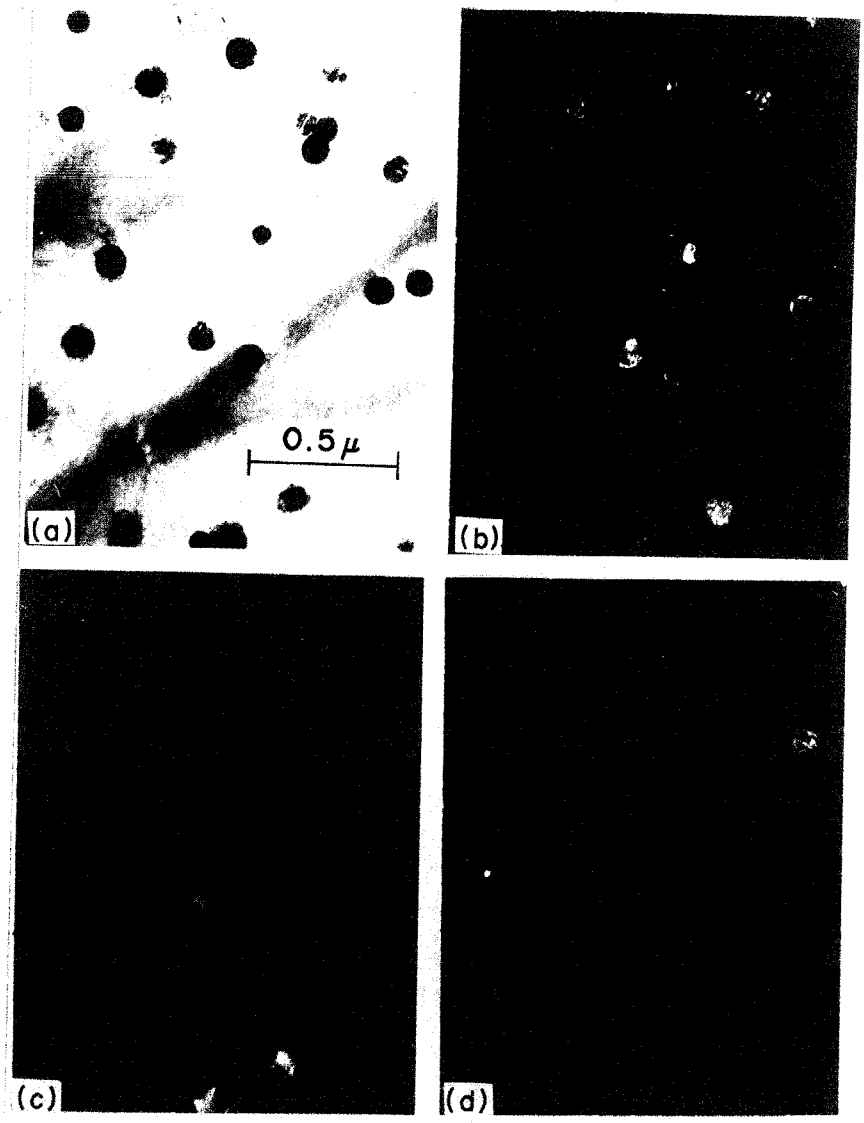

Fig.4.3

Electron micrographs showing the distribution of variants in $(1\bar{1}1)_f$ plane of a tensile specimen. (a) is a bright field image and (b), (c) and (d) are dark field images corresponding to the variants 1-6, 1-3 and 1-1, respectively.

twins could be observed in many particles of various sizes. Typical appearances of the banded structures in α-iron particles of various sizes are shown in Fig.4.4. One can see in Fig.4.4 that the number of the bands in the particle increases as the particle size becomes larger. About fifty α-iron particles of various sizes were examined and the number of bands in each particle is plotted against the particle diameter in Fig.4.5. It can be seen that the number of bands has the tendency to be proportional to the particle diameter despite of the large scatter in the observation. This will be discussed later.

4-4. Discussion

4-4-1. Stress effect on the $\gamma \rightarrow \alpha$ transformation in the iron particles.

As seen in Table 4.1, the sense of the applied stress plays an important role in the $\gamma \rightarrow \alpha$ martensitic transformation. This means a strong effect of the applied stress on the transformation. In Chapter 2,we have observed the variants of stress-induced martensite in Fe-23Ni-5Cr alloy single crystals and concluded that the applied stress aids the shear deformation of $\{111\}_f\langle 211\rangle_f$ in the initial stage of the transformation. In a similar manner, one can interpret the present experimental observation on the stress effect on the orientation of preferentially formed martensites.

The variants distribution shown in Table 4.1 is essentially the same as that found in the Fe-23Ni-5Cr alloy with almost the same stress axis (see Table 2.2). Moreover, Higo et al[3] observed the similar distribution of the stress-induced martensite in Fe-18Cr-14Ni stainless steel single crystals except that their observed distribution belonged to the variants, of which the orientation relationships were described with the plane parallel to the active

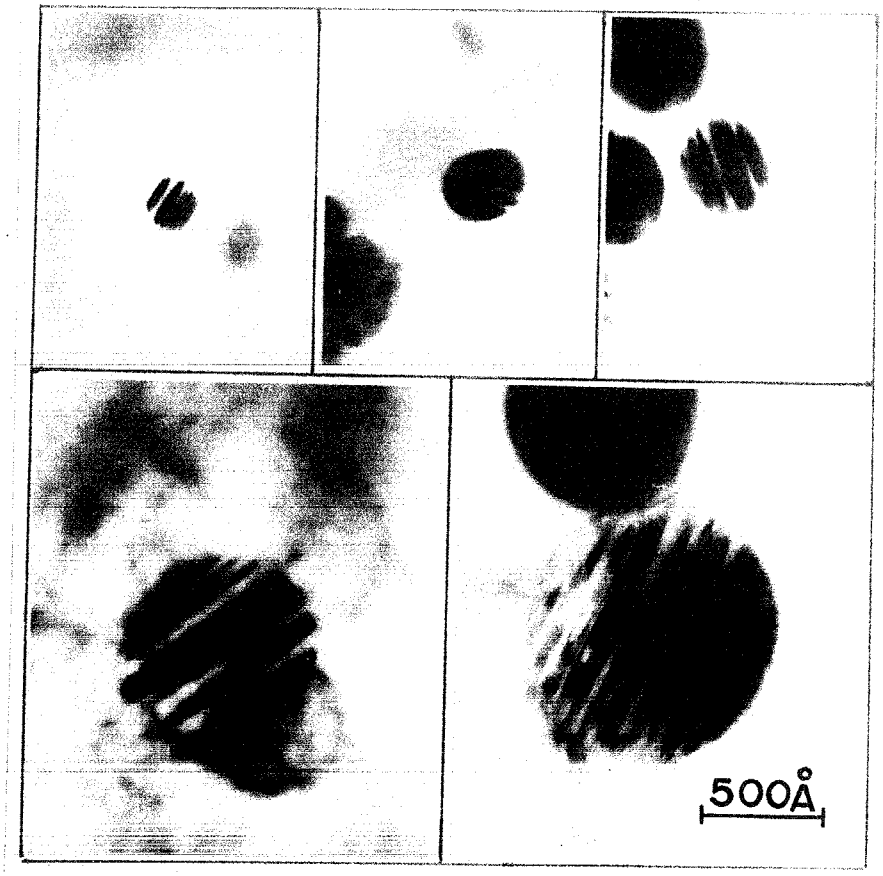

Fig.4.4

Typical banded structures varying with the size of the α-Fe particles.

Table 4.1 $\{111\}_f\langle 211\rangle_f$ shear mechanism and E_I/σ values of the 24 K-S variants with respect to the present stress axis. Observed frequency of the stress-induced martensite variants is listed in the right columns.

Variant notation		$\{111\}_f\langle 211\rangle_f$ shear mechanism		E_I/σ value	Observed frequency	
		1st shear	2nd shear		Tension	Compression
1	- 1	Bα(-0.343)	Cδ(-0.321)	0.028	—4%	—69%
	- 2	Bα(-0.343)	Dγ(-0.049)	-0.027		
	- 3	Cα(-0.143)	Dβ(0.186)	-0.078	—60%	
	- 4	Cα(-0.143)	Bδ(-0.061)	0.028		—65%
	- 5	Dα(0.481)	Bγ(0.011)	-0.027		
	- 6	Dα(0.481)	Cβ(-0.004)	-0.078	—65%	
2	- 1	Cδ(-0.321)	Bα(-0.343)	0.028		—42%
	- 2	Cδ(-0.321)	Aβ(-0.179)	-0.027		
	- 3	Bδ(-0.061)	Aγ(0.039)	-0.078		
	- 4	Bδ(-0.061)	Cα(-0.143)	0.028		—25%
	- 5	Aδ(0.390)	Cβ(-0.004)	-0.027	—31%	
	- 6	Aδ(0.390)	Bγ(0.011)	-0.078		
3	- 1	Aβ(-0.179)	Dγ(-0.049)	0.028		
	- 2	Aβ(-0.179)	Cδ(-0.321)	-0.027		
	- 3	Dβ(0.186)	Cα(-0.143)	-0.078	—10%	
	- 4	Dβ(0.186)	Aγ(0.039)	0.028		
	- 5	Cβ(-0.004)	Aδ(0.390)	-0.027		
	- 6	Cβ(-0.004)	Dα(0.481)	-0.078	—33%	
4	- 1	Dγ(-0.049)	Aβ(-0.179)	0.028	—19%	
	- 2	Dγ(-0.049)	Bα(-0.343)	-0.027		—9%
	- 3	Aγ(0.039)	Bδ(-0.061)	-0.078		
	- 4	Aγ(0.039)	Dβ(0.186)	0.028		
	- 5	Bγ(0.011)	Dα(0.481)	-0.027		—5%
	- 6	Bγ(0.011)	Aδ(0.390)	-0.078	>19%	

slip plane $(1\bar{1}1)_f$. In the present Cu-Fe alloy, the spherical martensite is formed. On the other hand, in the Fe-23Ni-5Cr and Fe-18Cr-14Ni alloys, the shapes of martensite are needle-like and lath-like, respectively. In short, the same variants of α-martensite are formed under the stress regardless of the martensite shape, when the change in lattice is from F.C.C. to B.C.C. This strongly suggests that one can interpret the present result on the stress effect on the preferential formation of the stress-induced martensite in a manner similar to that discussed in the studies of the Fe-23Ni-5Cr and Fe-18Cr-14Ni alloys. Accordingly, we can again conclude here that the applied stress aids the shear deformation of $\{111\}_f\langle 211\rangle_f$ in the $\gamma \rightarrow \alpha$ lattice change. In fact, the K-S variants with the large Schmid factors of the $\{111\}_f\langle 211\rangle_f$ shear systems are preferentially observed in Table 4.1.

One might argue that the applied stress determines the preferentially formed variants in such a manner that it aids the total deformation. This idea can be examined by calculating the interaction energy between the average Bain strain of the martensite and the applied stress, σ^A_{ij}. On the assumption that an α-iron particle consists of the same amount of two twin variants and that the elastic constants are uniform throughout the specimen, the interaction

energy per unit volume of martensite becomes

$$E_I = - \sigma^A_{ij} \varepsilon^*_{ij}$$

$$= - (\sigma\varepsilon^*_{11} \cos^2\alpha_1 + \sigma\varepsilon^*_{22} \cos^2\alpha_2 + \sigma\varepsilon^*_{33} \cos^2\alpha_3) , \qquad (4.1)$$

where σ is the applied stress, $\cos\alpha_i$ is a directional cosine between the stress axis ($\sim[416]_f$ in the present study) and the principal axis x_i of the F.C.C. lattice. ε^*_{ij} is the average transformation strain and can be written in the case of the twin variants 1-3 and 1-6 as

$$\varepsilon^*_{ij} = \frac{1}{2} (\overset{1}{\varepsilon}{}^*_{ij} + \overset{2}{\varepsilon}{}^*_{ij}) = \frac{1}{2} \begin{pmatrix} \varepsilon_2 & 0 & 0 \\ 0 & \varepsilon_1 & 0 \\ 0 & 0 & \varepsilon_1 \end{pmatrix} + \frac{1}{2} \begin{pmatrix} \varepsilon_1 & 0 & 0 \\ 0 & \varepsilon_2 & 0 \\ 0 & 0 & \varepsilon_1 \end{pmatrix} . \qquad (4.2)$$

With the lattice parameter of α-iron, 2.862 Å and that of γ-iron, 3.562 Å, which is an extrapolated value[41], ε_1 and ε_2 become 0.136 and -0.197, respectively. The calculated interaction energies are shown in terms of E_I/σ in Table 4.1. Positive and negative values of E_I/σ are favored in compression and in tension, respectively. We can see that twenty-four K-S variants are divided into the three sub-groups with the same E_I/σ values. However, the experimental results of the distribution of variants indicate that the variants belonging to the same sub-group were not observed equally even if we admit the statistical errors. This fact means that the formation of stress-induced martensite should not be understood solely through the stress effect on the total shape deformation.

Suzuki et al[29] discussed the formation of martensite during deformation and emphasized an important role played by internal stresses due to dislocations but not by applied stress. Since only the iron particles transform into martensite in the situation examined in the present study, only the dislocations, left around the particles, should be considered if one pursues the line adopted by Suzuki et al. However, in the present study, it was found that almost all the iron particles in the specimens deformed by 5 % shear at 77 K transform into martensite. 5 % shear was within the initial stage of work-hardening, where the flow curve does not exhibit the characteristics of strong particle bearing materials and the hardening rate is not significantly larger than that in pure copper, as shown in Fig.4.1. Thus, one should not expect the presence of Orowan loops which might have produced internal stresses on the iron particles. The remaining possibility is that some dislocation debris, which may play a role similar to that by statisti-

cally stored dislocations, is left around a particle. On this basis, however, it is hard to see that the distribution of the preferentially formed martensites is sensitive to the sense of the applied stress as observed in Table 3.1. Thus, it is concluded that the applied stress itself induces the martensitic transformation in the present study.

4-4-2. Elastic energy calculation

Instead of assigning the different Bain strains to the alternating regions constituting the banded structure, as implied by equation (4.2), the distribution of the eigenstrain in a twinned banded martensite particle Ω can be expressed as

$$\varepsilon^{T}_{ij} = {}^{1}\varepsilon^{T}_{ij} + {}^{2}\varepsilon^{T}_{ij}$$

$$= \begin{cases} \varepsilon^{T}_{ij}(0) + \frac{S}{2}\left(\delta_{i1}\delta_{j3} + \delta_{i3}\delta_{j1} \right), & (M = 0) \\ \varepsilon^{T}_{ij}(0) + \sum_{n=1}^{\infty} \bar{\varepsilon}^{T}_{ij}(n) \sin\left\{(2n-1)\pi\frac{M}{a}z\right\}, & (M \neq 0), \end{cases} \tag{4.3}$$

where z is the coordinate axis perpendicular to the twin plane, a the particle radius, 2M the number of the bands and δ_{ij} the Kronecker delta. Here, it is assumed that the alternating regions have equal thickness. The second term in (4.3) represents the twinning shear; for example, when M = 1 and the suitable coordinate axis is chosen, it becomes

$${}^{2}\varepsilon^{T}_{31} = {}^{2}\varepsilon^{T}_{13} = \begin{cases} \frac{S}{2} & (z > 0) \\ -\frac{S}{2} & (z < 0) \end{cases} \quad \text{in } \Omega,$$

with the other components being zero. Here, 2S = t is the twinning shear of B.C.C. metals, 0.707. Applying calculation given in 3-3-3 and assuming that the spherical precipitate and the matrix have the same isotropic elastic constants and the Poisson's ratio is 1/3, we can compute the elastic energy of a twinned martensite particle, due to the second term in (4.3). The results of M = 0 to 4 are shown in Fig.4.6, which is identical to Fig.3.4, where μ is the shear modulus. Although the calculation has not been performed for large values of M because of time limitation, it would be seen that as M increases, the elastic energy decreases, as speculated by Kinsman et al[44]. However, their calculation has been conducted in a limited case, corresponding to M = 1 in the present work and based on the rough expression of varying eigenstrain in the banded structure. Although it can be calculated easily by using the

Eshelby theory, the elastic energy due to the first term in equation (4.3), i.e., $\varepsilon_{ij}^{T}(0)$ is independent of the banded structure in the particle.

With respect to the above discussion, it should be useful to comment on a calculation performed by Easterling and Weatherly, who discussed the nucleation of martensite in a spherical particle[53]. They considered the uniform eigenstrains of expansion and shear and emphasized a difficulty in nucleation because of the large elastic energy due to the shear component. Although the model describing the structure of a martensite particle in their calculation is different from that in the present study, their calculation on nucleation must be modified. This is because the elastic energy can be reduced if the shear components are suitably distributed in many parallel regions, as it is the case.

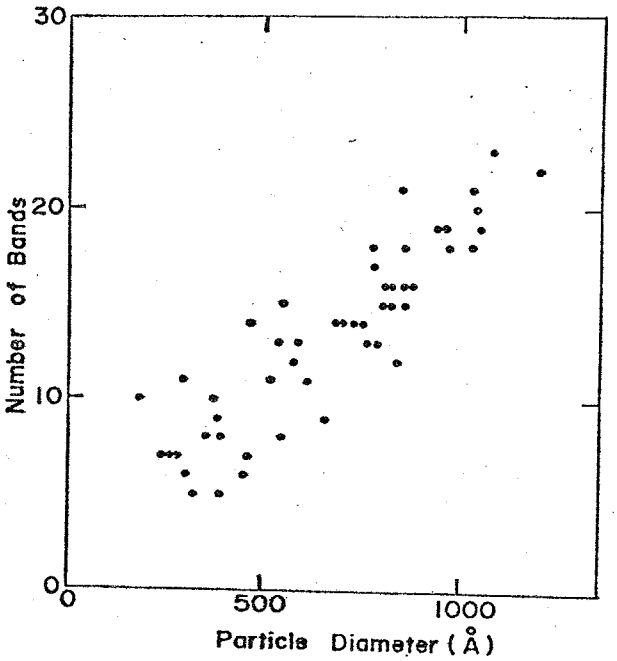

Fig.4.5

Relation between the particle size and the number of bands in the particle.

Here, it must be stressed that the elastic calculation employed in the present study is entirely different from that conducted by Shibata and Ono[43] and Easterling and Thölén[46]. For the eigenstrains (transformation strain plus lattice invariant strain) employed by them were uniform throughout a martensite. On the other hand, in the present study, the eigenstrain which changes periodically in the martensite was introduced. This makes it possible to take into account the effect of the non-uniform distribution of eigenstrain. Contrary to this, Shibata and Ono and Easterling and Thölén took the average eigenstrain which has, in reality, non-uniform distribution and thus, could not examine the effect of the fine structures such as designated by M in this study. In other words, the calculation using the average

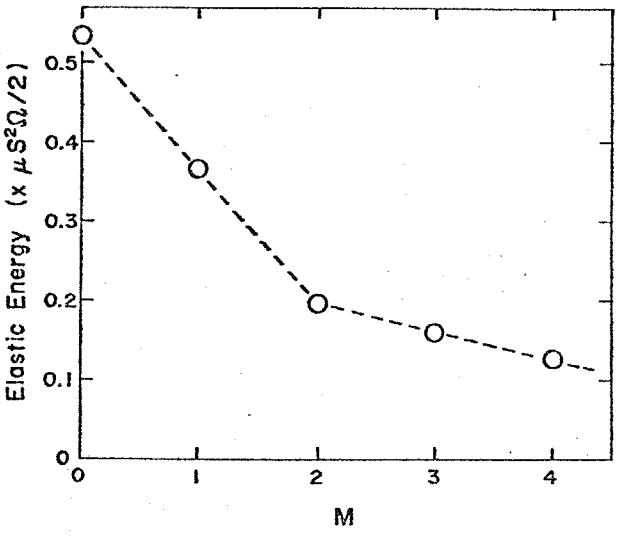

Fig.4.6

Elastic energy of a martensite particle with M pairs of twins.

eigenstrain considers, in essence, only the first term in equation (4.3), while the effect of the number of the twin bands is only taken into account by the second term in (4.3).

One might say that one can examine the possible existence of the lower elastic state by changing the relative volume of the two twin-related regions instead of assuming that the twinned layers have equal thickness. However, by symmetry consideration it can be shown that the elastic energy has a minimum when the spherical martensite is a single domain or consists of the equal amounts of two twin-related regions. Since it has been shown that the former situation results in the larger elastic energy, the assumption adopted in the elastic calculation is justified.

4-4-3. Banded structure in α-iron particles and twin-interface energy consideration.

As shown in Fig.4.5, the number of twin bands becomes larger as the particle becomes bigger. This can be examined by considering both the elastic and the twin-interface energies of a particle. In Fig.4.6, it is shown that the elastic energy is the decreasing function of M. However, if M increases, the interface of the twin boundary increases; the twin-interface energy is an increasing function of M. Therefore, it is not difficult to imagine that the sum of the elastic energy E_e and twin-interface energy E_t must have the minimum at a suitable value of $M = M_o$. This situation is schematically shown in Fig.4.7.

Let f(M) be the elastic energy per unit volume of a spherical α-iron martensite and Γ be the specific twin-interface energy per unit area. When $M \geq 1$, the total interface area A can be written as

$$A = 2 \sum_{n=0}^{M-1} \{\pi a^2 (1 - \frac{n^2}{M^2})\} - \pi a^2$$

$$= \pi a^2 (4M^2 - 1)/3M \ .$$

Accordingly, the sum of the elastic energy, pertinent to the present discussion, and the twin-interface energy becomes

$$E_e + E_t = \frac{4}{3} \pi a^3 f(M) + \frac{\pi \Gamma a^2}{3M} (4M^2 - 1) \ .$$

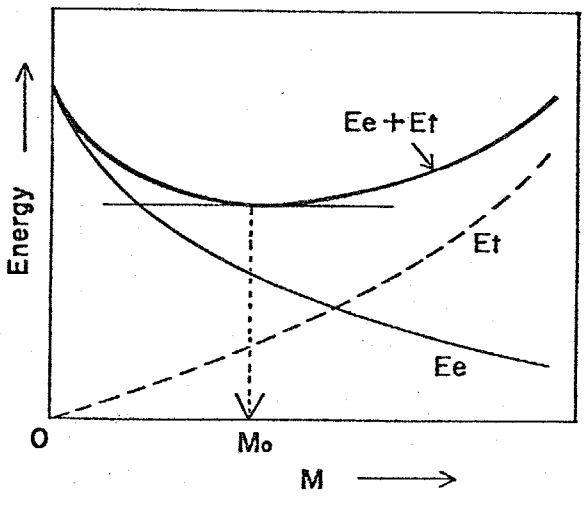

Fig.4.7

Schema of a dependence of the elastic (Ee) and the twin-interface (Et) energies of a martensite particle on the number of twin pairs, M. The sum of these two energies has a minimum at $M = M_o$.

Putting $M = M_o$ where the energy minimum is obtained, M_o can be expressed by solving

$$\left.\frac{\partial(E_e + E_t)}{\partial M}\right|_{M=M_o} = 0 ,$$

or

$$f'(M_o) = -\frac{\Gamma}{4a}\left(4 + \frac{1}{M_o^2}\right) .$$

considering that

$$4 < 4 + \frac{1}{M_o^2} \leqq 5 ,$$

the following expression can finally be obtained

$$|f'(M_o)| = \frac{\Gamma}{4a}\left(4 + \frac{1}{M_o^2}\right) \fallingdotseq \frac{\Gamma}{a} . \qquad (4.4)$$

Equation (4.4) means that $|f'(M_o)|$ is almost proportional to the inverse of the particle radius a. Noting that f(M) itself is a decreasing function, downward convex of M[†], one will see that as a becomes larger, M_o becomes larger, too. Thus, we can explain the experimental results shown in Fig.4.5 by considering both elastic and twin-interface energies of a particle.

Finally, let us evaluate the specific twin-interface energy by means of equation (4.4), Figs.4.5 and 4.6. In order to use the results of Fig.4.6, we must determine the particle radius at $M_o = 3$ (6 bands). From Fig.4.5, it can be chosen as $a \fallingdotseq 150$ Å. Figure 4.6 shows that $|f'(3)| = 0.033\mu S^2/2$. Substituting $\mu = 4.6 \times 10^{10}\ N/m^2$ and $S = 0.354$, we can obtain

$$\Gamma = a \cdot |f'(3)| \fallingdotseq 1.4\ J/m^2$$

Of course, this is a rough approximation because the graphical differentiation is inevitable in using Fig.4.6 and the assumption of the uniform and isotropic elastic constants is involved in the numerical calculation in addition to the numerical integration, as shown in 3-3-3. Furthermore, the estimated value of Γ is possibly an over-estimation. This is because the relation between M and a has been measured under the condition that the total energy is not minimized but goes to the minimum; for the twin formation is achieved by movement of twinning dislocations and this requires some amount of energy dissipation. In fact, Shibata and Ono[43] have shown that as the energy dissipation, E_d,

---

† This can duly be justified. For if f(M) should be the upward convex function of M, the elastic energy must become negative at very large values of M.

increases, the amount of the average lattice invariant shear to make $E_e + E_d$ minimum decreases. This is due to the fact that when the energy dissipation involved in the process, which seeks the equilibrium state, is not vanishing, the real physical system does not attain the equilibrium state which is required by the equilibrium thermodynamic law. For example, in the present situation, when the band of twins is formed, the generalized force, due to the decrease of the elastic energy and the increase of the twin-interface energy, is given by $-\partial(E_e + E_t)/\partial s$, where s represents a parameter to indicate the amount of twinning shear. The force to oppose the twin formation is $\partial E_d/\partial s$, where E_d is the energy dissipation due to the movement of the twinning dislocations. It is natural that the final state is attained when $\partial(E_e + E_t + E_d)/\partial s = 0$, if the energy dissipation is not zero. In the present situation, this means that the physically attained M is lower than M_o defined in (4.4). This is the correct understanding of the conclusion reached by Shibata and Ono[43].

However, the large value of Γ is not in contradiction to the general belief that the stacking fault energy as well as the twin-interface energy is large in α-iron. In fact, a calculation by Vítek[15] and one by Masuda[16] give large values of Γ. Furthermore, the absence of annealing twin in α-iron certainly supports the large value of Γ. It is noted that even in Al which is considered to have Γ of ~ 0.2 J/m^2, annealing twins are sometimes observed.

In concluding this section, it must be emphasized that the significant contribution of the twin-interface energy should be considered in the energetics involving martensitic transformation.

4-5. Conclusion

Spherical α-iron martensite in a copper matrix was obtained by applying the uniaxial tensile and compressive stresses on single crystals of a Cu-Fe alloy. The orientation of preferentially formed martensite variants under the applied stress was examined by the electron microscope, and was essentially the same as that of the preferentially formed martensites in an Fe-23Ni-5Cr and an Fe-18Cr-14Ni alloys. From this, it has been concluded that the applied stress plays an important role on the $\{111\}_f\langle 211\rangle_f$ shear systems in the initial stage of the transformation. Electron microscopic observation indicates that the α-iron particles are divided into the alternating twin bands, the number of which is strongly size dependent. Considering both the elastic and twin-interface energies of a particle, this size dependence can be explained and the specific twin-interface energy is evaluated to be ~ 1.4 J/m^2.

4-6. Addendum

(a) As will be shown in Chapter 5, a γ-iron particle in copper matrix is subject to a large elastic energy due to the misfit of lattice parameters between γ-iron and copper matrix. The resultant internal stress $\overset{s}{\sigma}_{ij}$ is tensile and hydrostatic, i. e. $\overset{s}{\sigma}_{ij} = \overset{s}{\sigma}\delta_{ij}$, and $\overset{s}{\sigma}$ can be evaluated to be 1600 MN/m^2. On the other hand, the magnitude of the tensile stress is the order of 50 MN/m^2 from Fig.4.1. From these values of the internal and external stresses, it can be shown that the work done by these stresses during the $\gamma \rightarrow \alpha$ transformation process in an iron particle becames respectively 1.2×10^8 J/m^3 (by the internal stress) and 3.8×10^6 J/m^3 (by the external stress) which is the largest value. These values mean that from the quantitative standpoint of view, the effect of the external stress on the transformation is negligible compared with that of the internal stress. However, the fact that the γ-iron particles transform into α-martensite only when the external stress is applied strongly indicates that not the huge hydrostatic inter--al stress but the shear stress is essential for the $\gamma \rightarrow \alpha$ transformation to occur.

(b) As mentioned in the third paragraph in Section 4-4 from p.48 to p.49, observed number of the twin bands is not larger than M_o. The significant scattering of the data points in Fig.4.5 may be caused by the existence of a variety of physical processes, which the present study neither intends to nor is able to pin down at this moment and by which the large elastic energy brought about by the insufficient number of the twin bands is relaxed. Pursuing this understanding, one is compelled to conclude that even the use of the largest number of M at a given particle size in Fig.4.5 gives the upper bound of Γ. If one uses the data point of (M=10, a=180 Å) in Fig.4.5 and extrapolates it linearly to M = 3, a becomes 60 Å. This combination, (M=3, a=60 Å), results in $\Gamma \leq \sim 0.6$ J/m^2. It is interesting that $\Gamma = 0.6$ J/m^2 is very close to Γ calculated by Vítek[15] and Masuda[16].

CHAPTER 5

ORIENTATION AND SHAPE DEPENDENCE OF ELASTIC ENERGY OF ELLIPSOIDAL PRECIPITATES IN ANISOTROPIC MEDIA

5-1. Motivation of the Study

In a Cu-Fe alloy, the shape of γ-iron precipitates formed during aging is spherical, as shown in Chapter 4. On the other hand, disc-shaped copper precipitates, usually called G.P. zones, are observed in an Al-Cu alloy. These two types of precipitates have the identical eigenstrain (transformation strain) in quality with some differences in quantity and in elastic constants of the matrix and the precipitates. It is conceivable that elastic energy depending on the eigenstrain as well as on the elastic constants plays a role in determining the shape and orientation of the precipitates.

The shape dependence of the precipitation was first discussed by Nabarro [56]. He considered three types of shapes (disc, needle and sphere) of precipitates and concluded that the disc-shaped precipitate has the smallest elastic energy, while the spherical one has the largest. Later, Laszlo pointed out that the conclusion reached by Nabarro could not be taken for granted[57]; it is valid only when the shear modulus of the precipitate is smaller than that of the matrix, but the reverse condition is correct if the precipitates are larger in shear modulus than the matrix.

However, the calculations conducted by Nabarro and Laszlo are based on isotropic elasticity. Recent developments on the elastic state of an ellipsoidal inclusion in an anisotropic medium can be used to evaluate the elastic energy due to precipitation occurring in actual and real alloys which have anisotropic elastic constants. Only very recently, a single paper has appeared which has calculated the elastic energy of precipitates in some crystals with anisotropic elasticity[58]. Since such a calculation inevitably involves some numerical computations, the above paper alone does not offer the universal condition, which is similar to that by Nabarro and Laszlo in isotropic elasticity and on which the shape and orientation dependence of precipitation in any alloy can be discussed.

Thus, it has been decided that the elastic energy of precipitates of representative shapes is calculated in a Cu-Fe alloy to pursue the curiosity arising from the observed shape of γ-iron precipitates surrounded by copper matrix. For comparison, a similar calculation is conducted in an Al-Cu alloy.

It is well known that if a precipitate and a matrix have identical

isotropic elastic constants with the eigenstrain (misfit strain) of $\varepsilon^*_{ij} = \varepsilon\delta_{ij}$, the elastic energy does not depend on the shape and that this is due to the absence of the interaction between any volume elements constituting the particle. Thus, if the elastic energy depends on the shape and orientation of the precipitate in an anisotropic medium, one can conclude that the interaction among constituting volume elements is present and accounts for such shape and orientation dependences. The calculation of the elastic interaction energy between two volume elements requires the stress field outside of a volume element. Recently, Mura and Cheng[21] have succeeded to formulate the elastic field outside of an ellipsoidal inclusion in an anisotropic medium in a usable form. This has enabled the present study to examine the shape and orientation dependence of the elastic energy of the precipitate by the interaction between the constituting elements.

5-2. Elastic Energy of a Spherical-, Needle- or Disc-Shaped Precipitate in an Anisotropic Medium

It has been shown[20,39] that when a homogeneous ellipsoidal inclusion

$$x_1'^2/a_1^2 + x_2'^2/a_2^2 + x_3'^2/a_3^2 \leq 1 \tag{5.1}$$

has constant eigenstrains of ε^*_{mn}, total strains (constrained strain) γ_{ik} inside it is uniform and is given by

$$\gamma_{ik} = S_{ikmn}\varepsilon^*_{mn} \tag{5.2}$$

with

$$S_{ikmn} = \frac{a_1a_2a_3}{8\pi}\int_{S^2} C_{j\ell mn}\,\bar{\xi}_\ell\{\bar{\xi}_k N_{ij}(\underset{\sim}{\bar{\xi}}) + \bar{\xi}_i N_{kj}(\underset{\sim}{\bar{\xi}})\}D^{-1}(\underset{\sim}{\bar{\xi}})\zeta^{-3}(\underset{\sim}{\bar{\xi}})\,dS(\underset{\sim}{\bar{\xi}}) \,. \tag{5.3}$$

Here $C_{j\ell mn}$ are the elastic constants, $\underset{\sim}{\bar{\xi}}$ is the unit vector and the integration is performed on the unit sphere S^2. $N_{ij}(\underset{\sim}{\bar{\xi}})$ and $D(\underset{\sim}{\bar{\xi}})$ are respectively the cofactors and the determinant of the 3×3 matrix with elements $C_{ipjq}\bar{\xi}_p\bar{\xi}_q$ as (i,j) components and $\zeta(\underset{\sim}{\bar{\xi}})$ is given by

$$\zeta = \{a_1^2(e_{j1}\bar{\xi}_j)^2 + a_2^2(e_{j2}\bar{\xi}_j)^2 + a_3^2(e_{j3}\bar{\xi}_j)^2\}^{1/2} \tag{5.4}$$

where $e_{j\ell}$ is the direction cosine between the x_j axis (taken as the crystallographic axis such as [100], [010] and [001]) and x'_ℓ axis, parallel to the principal axis of the ellipsoid, (5.1). When $a_1 = a_2$ and $a_3/a_1 \to \infty$ (needle), it can be shown that (5.3) reduces to[20]

$$S_{ikmn} = \frac{1}{4\pi} \oint_{S^1} C_{j\ell mn} \bar{\xi}_\ell \{\bar{\xi}_k N_{ij}(\underset{\sim}{\bar{\xi}}) + \bar{\xi}_i N_{kj}(\underset{\sim}{\bar{\xi}})\} D^{-1}(\underset{\sim}{\bar{\xi}}) dL(\underset{\sim}{\bar{\xi}}) \ , \qquad (5.5)$$

where the integration is performed along the unit circle, S^1, the plane bounded by it being perpendicular to the x_3' axis (needle axis). Similarly, when $a_1 = a_2$ and $a_3/a_1 \to 0$ (disc), it has been shown[20,36] that

$$S_{ikmn} = \frac{1}{2} C_{j\ell mn} \bar{\xi}_\ell \{\bar{\xi}_k N_{ij}(\underset{\sim}{\bar{\xi}}) + \bar{\xi}_i N_{kj}(\underset{\sim}{\bar{\xi}})\} D^{-1}(\underset{\sim}{\bar{\xi}}) \ , \qquad (5.6)$$

where the unit vector, $\underset{\sim}{\bar{\xi}}$, is perpendicular to the disc plane ($\underset{\sim}{\bar{\xi}} // x_3'$).

If the inhomogeneous inclusions with the elastic constants of C^*_{pqik} and the eigenstrain of ε^{**}_{mn} is dealt with, the stress σ_{pq} and the strain γ_{ik} in the inclusion are found by solving the following linear equations:

$$\sigma_{pq} = C_{pqik}(\gamma_{ik} - \varepsilon^*_{ik}) = C^*_{pqik}(\gamma_{ik} - \varepsilon^{**}_{ik}) \qquad (5.7)$$

with (5.2) $\sim$ (5.6). The above equation is obtained by considering the equivalency of the stress and the strain of the inhomogeneous inclusion and the equivalent homogeneous inclusion[19]. As often utilized, the elastic energy, E_s, due to the inclusion is given by

$$E_s = -\frac{1}{2} \int_{V_o} \sigma_{pq} \varepsilon^{**}_{pq} \, d\underset{\sim}{x} = -\frac{1}{2} V_o \sigma_{pq} \varepsilon^{**}_{pq} \ , \qquad (5.8)$$

where V_o denotes the volume of the inclusion. Since (5.3) is not in general integrated analytically, one has to perform the pertinent calculation numerically, by choosing adequate values of the elastic constants which depend on particular materials. Choices of materials are numerous and general discussion on the elastic state of the precipitates is hard to conduct. Thus, in this study, restriction will be put on a case which is pertinent to the present thesis and will be discussed later.

For simplicity, we will deal with the case of $\varepsilon^{**}_{mn} = \varepsilon\delta_{mn}$, corresponding to the situation where the substitutional solute atoms coagulate or form precipitates with the crystal structure identical to that of the matrix but different elastic constants. Also copper is selected as the matrix material, with $C_{1111} = 16.84$, $C_{1122} = 12.14$ and $C_{1212} = 7.54 \times 10^{10}$ N/m^2. The numerical integration of (5.3) is performed by a computer.

5-2-1. Orientation dependence of the elastic energy due to a needle- or disc-shaped precipitate.

Figures 5.1 and 5.2 show the equi-energy contours with respect to the

Needle (10^{10} J/m^3)

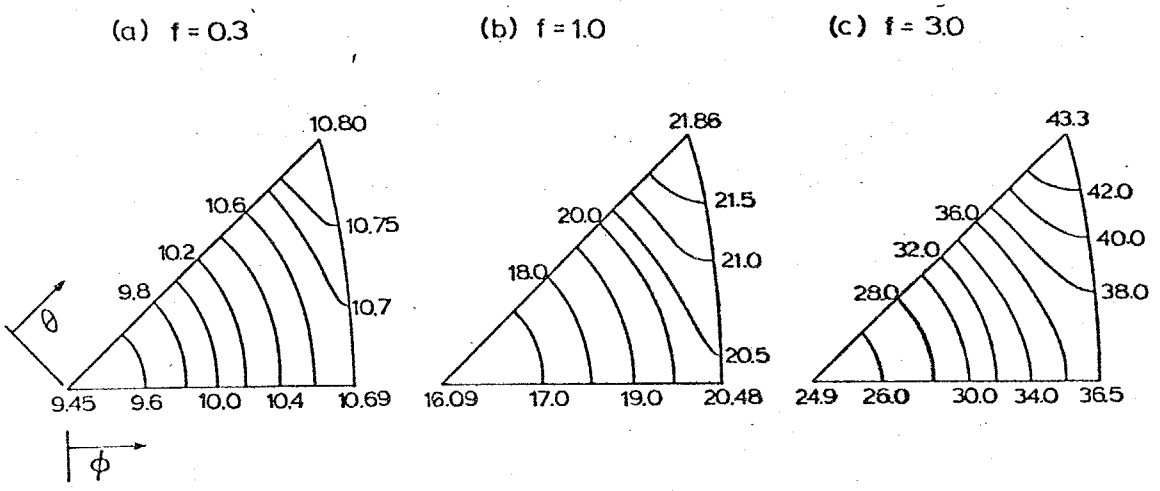

Fig.5.1

Elastic energy of a needle shaped precipitate as a function of orientation in copper (10^{10} J/m^3)

Disc (10^{10} J/m^3)

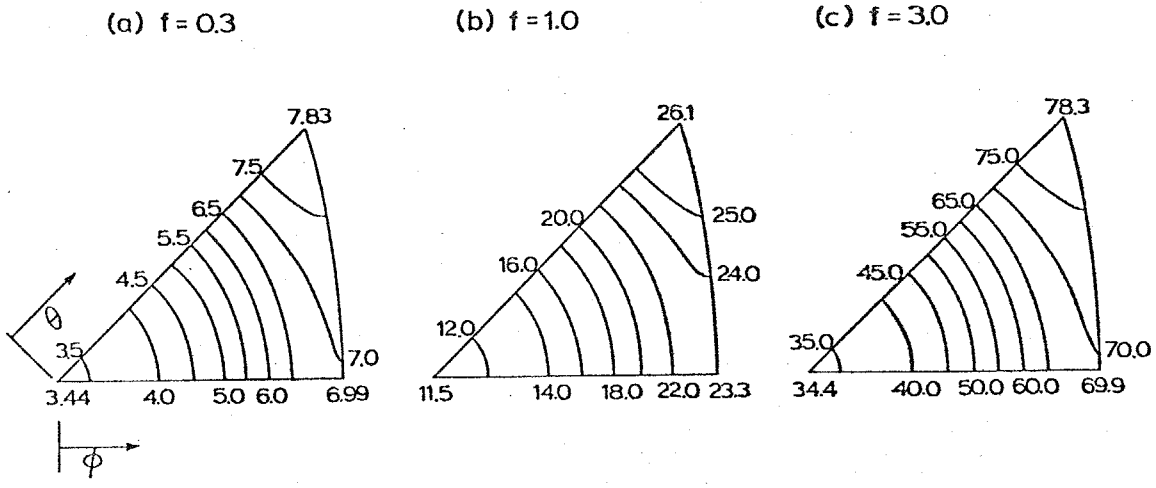

Fig.5.2

Elastic energy of a disc shaped precipitate as a function of orientation in copper (10^{10} J/m^3)

principal axes of the copper matrix in the case of $C^*_{pqik} = f\,C_{pqik}$ with f = 0.3, 1 and 3 for a needle and a disc, respectively. It is seen that the minimum elastic energy is attained when the needle axis is parallel to [001] and the disc plane is perpendicular to [001]. The elastic energy becomes maximum when the needle is parallel to [111] and the disc plane is perpendicular to [111]. The identical orientation dependence of the elastic energy has been found for f = 0.1 to 10.

5-2-2. Shape dependence of the elastic energy

In Fig.5.3, the elastic energy of a spherical precipitate is plotted against f together with those of a needle and a disc precipitates at the lowest energy orientation. When f is small, say less than 1, the elastic energy is the smallest in the disc and the largest in the sphere, although the difference between the sphere and the needle is not large. When f is large, the sequence in the elastic energy becomes inversed. The cross point is somewhere around f = 2 ∿ 3. These results are similar to those obtained by the isotropic elasticity[57]. However, the essential difference between the present anisotropic calculation and the previous isotropic calculation exists in that the three curves do not cross together in the former, while, in the latter, they cross together at f = 1.0.

Although they are not known, the elastic constants of γ-iron are considered to be of the same order or at most less than twice of those of copper. Thus, the iron precipitates in a copper matrix could decrease the elastic energy if they took a shape of a needle or a disc. This argument can be examined by using the elastic constants of iron-base F.C.C. alloys which are believed to be not much different from the F.C.C. iron. For example, an F.C.C. alloy of 70%Fe-30%Ni has been reported to have C^*_{1111} = 14.45, C^*_{1122} = 8.67 and C^*_{1212} = 11.34 × 10^{10} N/m^2[59]. Also the elastic constants of 70%Fe-18%Cr-12%Ni (austenitic stainless steel) are available[60], C^*_{1111} = 19.11, C^*_{1122} = 11.78 and C^*_{1212} = 13.85 × 10^{10} N/m^2. The elastic energy,

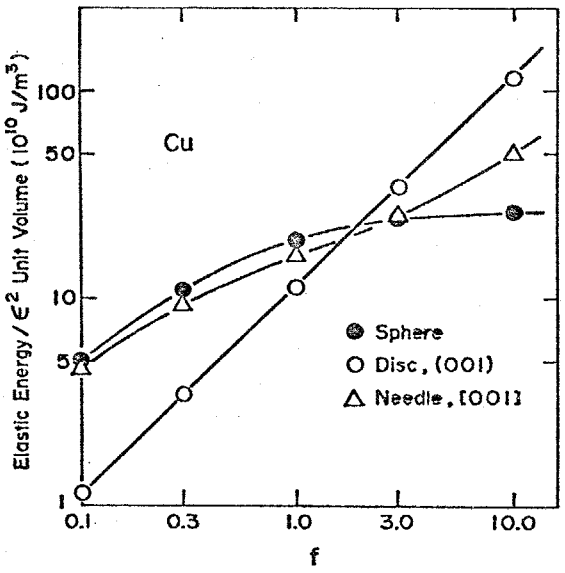

Fig.5.3

Elastic energy of spherical, disc and needle precipitates as a function of relative elastic constants f (copper matrix)

thus calculated by using these elastic constants and assigned to unit volume of a precipitate with $\varepsilon = -0.0125$[41] is 27.4×10^6 J/m^3(sphere), 23.9×10^6 J/m^3(needle) and 19.8×10^6 J/m^3(disc) for the elastic constants of 70%Fe-30% Ni and 30.2×10^6 J/m^3(sphere), 27.0×10^6 J/m^3(needle) and 25.5×10^6 J/m^3 (disc) for those of austenitic stainless steel. The elastic energies of the needle and the disc are minimum when they lie parallel to [001] and (001), respectively. Thus, the calculation based on the available elastic constants of ferrous F.C.C. alloys also gives the identical argument that spherical iron precipitates are not the favorable ones in terms of elastic energy. However, the interfacial area between the matrix and a needle or a disc is much larger than that between a sphere and the matrix when the volume is constant.

Consequently, when ε is small or when the interfacial enery is large, one could expect that γ-iron precipitates take a form of sphere. Although the interfacial energy between copper and γ-iron is not known, ε is, in fact, certainly small, -0.0125[41].

In connection with the above discussion, similar calculation using aluminum as a matrix is performed. The elastic constants of aluminum are $C_{1111} = 10.82$, $C_{1122} = 6.13$ and $C_{1212} = 2.85 \times 10^{10}$ N/m^2. Figure 5.4 shows the calculated results, similar to Fig.5.3, with aluminum as a matrix material. Again in this case, a needle and a disc precipitates take a minimum elastic energy when they lie parallel to [001] direction and (001) plane, respectively.

Contrary to the γ-iron precipitates in a Cu-Fe alloy, disc-shaped copper precipitates are formed in an Al-Cu alloy. One can also understand this facts through the elastic energy consideration. Using the elastic constants of copper (a precipitate) and aluminum (a matrix) with $\varepsilon = -0.109$ (calculated from the lattice parameters of copper and aluminum), the elastic energy assigned to unit volume of a copper precipitate is calculated as 14.9×10^8 J/m^3(sphere), 14.4×10^8 J/m^3(needle) and 13.6×10^8 J/m^3(disc). The elastic energies of the needle and the disc are minimum when they lie parallel to [001] and (001), respectively. Thus, one can

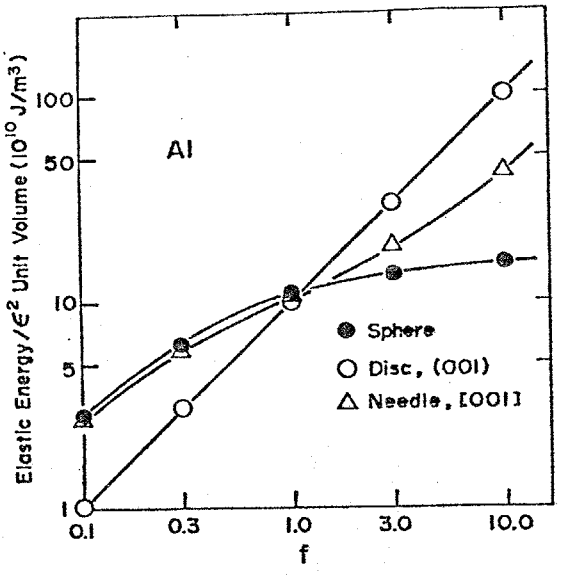

Fig.5.4

Elastic energy of spherical, disc and needle precipitates as a function of relative elastic constants f (aluminum matrix)

see that the copper precipitates take the form of disc in an Al-Cu alloy. Of course, one must consider the effect of the interfacial energy between the precipitates and the matrix. However, in an Al-Cu alloy, the difference of the elastic energies between the sphere and the disc is about two figures larger than that in a Cu-Fe alloy. This is entirely due to the large value of ε in an Al-Cu alloy and the interfacial energy contribution can duly be neglected.

5-3. Interaction Between Elements Constituting Precipitates

The results in Figs.5.1 ~ 5.3 will be discussed in a slightly different manner. Let us consider a homogeneous inclusion for simplicity. The fact that the elastic energy depends on the shape and orientation is a characteristic of the presence of anisotropy in elastic constants and indicates that there is an interaction among particles which constitute the precipitate. The interaction energy between two particles with volumes V_1 and V_2 is expressed as

$$E_I = - \int_{V_2} {}^{1}\sigma_{pq} \, {}^{2*}\varepsilon_{pq} \, d\underset{\sim}{x} \, , \tag{5.9}$$

where ${}^{1}\sigma_{pq}$ is the stress due to particle 1 and ${}^{2*}\varepsilon_{pq}$ is the eigenstrain of particle 2. The stress field outside of an ellipsoidal particle has been given by Mura and Cheng[21] in the case of constant ε^*_{mn} as

$$\sigma_{pq}(\underset{\sim}{x}) = C_{pqik} \left\{ \frac{a_1 a_2 a_3}{8\pi^2} \varepsilon^*_{mn} \int_{S^*} C_{j\ell mn} \bar{\xi}_\ell \bar{\xi}_k N_{ij}(\underset{\sim}{\bar{\xi}}) D^{-1}(\underset{\sim}{\bar{\xi}}) \zeta^{-3}(\underset{\sim}{\bar{\xi}}) dS(\underset{\sim}{\bar{\xi}}) \right.$$

$$\left. - \frac{\varepsilon^*_{mn}}{2\pi} \oint_L C_{j\ell mn} \bar{\xi}_\ell \bar{\xi}_k N_{ij}(\underset{\sim}{\bar{\xi}}) D^{-1}(\underset{\sim}{\bar{\xi}}) y^{-1} d\theta(\underset{\sim}{\bar{\xi}}) \right\} \, , \tag{5.10}$$

Here , $\underset{\sim}{\bar{\xi}}$ is a unit vector, $y = (y_i y_i)^{1/2}$ and $\underset{\sim}{\bar{\zeta}}$ and $\underset{\sim}{y}$ are defined as

$$\left.\begin{aligned} &y_1 = x_1/a_1 \, , \quad y_2 = x_2/a_2 \, , \quad y_3 = x_3/a_3 \, , \\ &\bar{\zeta}_1 = a_1\bar{\xi}_1/\zeta, \quad \bar{\zeta}_2 = a_2\bar{\xi}_2/\zeta, \quad \bar{\zeta}_3 = a_3\bar{\xi}_3/\zeta, \\ &\zeta^2 = (a_1\bar{\xi}_1)^2 + (a_2\bar{\xi}_2)^2 + (a_3\bar{\xi}_3)^2 \, . \end{aligned}\right\} \tag{5.11}$$

S^* is the subdomain on S^2 satisfying

$$\underset{\sim}{\bar{\zeta}} \cdot \underset{\sim}{y} \leq 1 \tag{5.12}$$

and the integral along L is performed along the circle on S^2 given by

$$\bar{\underset{\sim}{\zeta}} \cdot \underset{\sim}{y} = 1 \qquad (5.13)$$

Thus, by performing the integration in (5.10) numerically, one can calculate the interaction energy between two ellipsoidal particles, once their positions are specified.

Suppose a needle-shaped precipitate is formed by adding solute particles along a particular direction. The energy required to form such a row of particles is the self energy plus the interaction energy of the solute particles, considered as misfitting spheres. Since the self energy is independent of the direction, one can tell the energetically favorable direction of the row of particles by examining their interaction energy. Tables 5.1 and 5.2 show the interaction energy between two spheres with $\varepsilon^*_{mn} = \delta_{mn}$ along the relative direction between them. Here, the distance R between the two particles is normalized by a radius of sphere. It should be emphasized that the interaction energy vanishes for isotropic media and, therefore, these values of the energy in Tables come from the anisotropy of the material. By comparing the magnitude of the interaction energy at a given R/a along [001] ($\phi = 0°$), [011] ($\phi = 45°$) and [111] ($\theta = 54.7°$), it is certainly understood that [001] is the most favorable direction and [111] the least favorable one. This leads to the same conclusion obtained from Fig.5.1 that a needle-shaped precipitate will be formed in [001] direction.

The interaction energy averaged over ϕ is also listed in Table 5.1. Compare this with the interaction energy at $\phi = 0°$. Then, it will be seen that a disc precipitate perpendicular to [001] has the lower energy than a needle precipitate parallel to [001] (see Fig.5.3). At the identical R, the interaction energy along [001] is smaller than that averaged over ϕ. However, one has to compare these values in the situation where the equal number of the solute atoms are accumulated. This can be done by comparing the interaction

Table 5.1 Interaction energy of two spherical particles in Cu with $\varepsilon^*_{ij} = \delta_{ij}$. ϕ is defined in Fig.5.1. Energy is normalized by dividing the particle volume and is in units of J/m^6.

R/a \ ϕ	0°	11.3°	22.5°	33.8°	45.0°	Average
2	-3.731×10^{10}	-3.195×10^{10}	-1.488×10^{10}	2.663×10^{9}	9.039×10^{9}	-1.449×10^{10}
4	-4.746×10^{9}	-4.440×10^{9}	-3.391×10^{9}	4.280×10^{8}	3.392×10^{9}	-1.752×10^{9}
8	-7.755×10^{8}	-6.574×10^{8}	-5.091×10^{8}	-2.365×10^{7}	5.622×10^{8}	-2.801×10^{8}
16	-1.967×10^{8}	-1.496×10^{8}	-9.143×10^{7}	-2.190×10^{7}	6.161×10^{7}	-7.960×10^{7}
32	-7.464×10^{7}	-5.513×10^{7}	-2.689×10^{7}	-1.122×10^{7}	1.978×10^{5}	-3.354×10^{7}

Table 5.2 Interaction energy of two spherical particles in Cu with $\varepsilon^{*}_{ij} = \delta_{ij}$. θ is defined in Fig.5.1.

R/a \ θ	0°	13.7°	27.4°	41.1°	54.7°
2	-3.731×10^{10}	-2.913×10^{10}	-4.652×10^{10}	1.819×10^{10}	2.619×10^{10}
4	-4.746×10^{9}	-4.017×10^{9}	-2.444×10^{9}	2.690×10^{9}	5.794×10^{9}
8	-7.755×10^{8}	-3.405×10^{8}	-2.462×10^{8}	4.106×10^{8}	8.827×10^{8}
16	-1.967×10^{8}	3.964×10^{7}	3.734×10^{7}	1.119×10^{8}	1.410×10^{8}
32	-7.464×10^{7}	4.611×10^{7}	4.001×10^{7}	4.551×10^{7}	3.151×10^{7}

energy at the square of R for the needle with that at R for the disc.

5-4. Conclusion

In this chapter, it has been shown that the elastic field and energy of a precipitate can be treated with anisotropic elasticity and that the shape dependence of the precipitates can be interpreted in terms of the interaction energy between constituting elements. The elastic energy of a precipitate with misfit strains depends on both the shape and the direction with respect to the matrix crystalline axes. When the elastic constants of a precipitate are smaller than those of a matrix, the elastic energy is the smallest in a disc and the largest in a spherical precipitate. On the other hand, when the elastic constants of a precipitate are larger than those of a matrix, the shape dependence of the elastic energy becomes reversed. Orientation dependence of the elastic energy coming from the anisotropic elasticity indicates that the needle- and disc-shaped precipitates prefer to form parallel and perpendicular to [001], respectively. These facts can equally well be explained in terms of the interaction energy between two particles.

CHAPTER 6

SUMMARY AND CONCLUDING REMARKS

In this study, the effect of applied stress on F.C.C. to B.C.C. martensitic transformation in Fe-23Ni-5Cr and Cu-1.06Fe single crystals has experimentally been studied. Here, the orientations of the martensites, preferentially formed under stress, have been determined with respect to the direction and sense of applied stress. This is to discuss the operation of the atomic shear system to induce the lattice change. In addition, the elastic calculations, based on the recent development of the elastic state of an ellipsoidal inclusion, have been conducted to discuss several aspects of the present study; the evaluation of elastic state of a disc and a spherical martensite and the calculation of the elastic energy associated with precipitation in a Cu-Fe alloy.

The content of this thesis and the important findings in the present study are summarized as follows :

In Chapter 1, of Introduction, the historical backgrounds and the motivations of the present studies were mentioned.

In Chapter 2, the experimental study on the effect of applied stress on F.C.C. to B.C.C. martensitic transformation in Fe-23Ni-5Cr single crystals was presented. The crystallographic analyses of the stress-induced martensite indicate the important role of the applied stress in the initial stage of the transformation involving the lattice change. On the contrary, the experimental observations could not rationally explain the effect of the applied stress on the total shape deformation of martensite.

In Chapter 3, the elastic energy associated with the transformation was evaluated by conducting the calculation based on the elastic state in an inclusion with periodically distributed eigenstrains. It has been found that if one duly takes into account the periodical distribution of eigenstrains in a real martensite, a significant amount of the elastic energy does exist. This fact implies that the basic concepts of the phenomenological crystallographic theory should be re-examined and that the energetics involving the martensitic transformation should be considered by taking into account the importance of the periodical distribution of eigenstrains in a real crystal.

In Chapter 4, the effect of applied stress on F.C.C. to B.C.C. martensitic transformation in spherical iron precipitates was examined by using Cu-1.06Fe alloy single crystals. Together with the results in Chapter 2, it has been

concluded that the applied stress mainly affects the $\{111\}_f\langle 211\rangle_f$ shear systems in the lattice change. In addition, by using the calculated result in Chapter 3, the specific twin-interface energy in α-iron was evaluated.

In Chapter 5, the orientation and shape dependence of precipitates was examined by using the elastic calculations in an anisotropic medium. Special interests were placed upon the interaction energy between the volume elements constituting the particles. From the calculated results, difference in shape of the precipitates in different materials, such as a spherical precipitation of iron in a Cu-Fe alloy and a disc-shaped precipitation of copper in an Al-Cu alloy (G.P. zone), can be explained by considering the elastic state associated with these precipitations.

As Chapter 1 clearly shows, the mechanics associated with the martensitic transformation has been discussed on the basis of the phenomenological theory by most research groups. Contrary to this, the present study has tried to seek, by studying the transformation under stress, the deformation which induces the lattice change. The difficulty for the phenomenological theory to account for the experimental observations made in the present study has been pointed out. To emphasize this point, the transformation of spherical iron particles, which are of the shape outside of the phenomenological theory, has been studied in addition to an iron-base alloy. Furthermore, it has been shown by the elasticity calculations that the basis of the fundamental concept or assumption of the phenomenological theory is never taken for granted.

APPENDIX A

Derivation of the Fundamental Equation (3.3)

Appendices A and B come from the paper which bears the names of Mura, Mori and myself[17]. The paper consists of the derivation of the fundamental equations, mainly developed by Mura and Mori and the applications exploited by me to evaluate the elastic states of some martensites which are put in Chapter 3. Since the fundamental equations and their derivations are important for this thesis and would certainly help the readers understand the background development, the present and following appendices are spared to them.

The displacement component u_i in an indefinitely-extended medium caused by a distribution of eigenstrain $\varepsilon^*_{ij}(\mathrm{x})$ in a domain Ω can be expressed by the following Volterra form

$$u_i(\mathrm{x}) = -(2\pi)^{-3} \frac{\partial}{\partial x_l} \int_\Omega d\mathrm{x}' \int_0^\infty \xi^2\, d\xi \int_{S^2} C_{jlmn} \varepsilon^*_{mn}(\mathrm{x}')(N_{ij}(\xi)/D(\xi)) \times \exp\{i\xi\cdot(\mathrm{x}-\mathrm{x}')\}\, dS(\bar{\xi}), \quad (1)$$

where $d\mathrm{x}' = dx'_1\, dx'_2\, dx'_3$, C_{ijkl} are elastic constants, S^2 is the unit sphere $\bar{\xi}_i\bar{\xi}_i = 1$, and $N_{ij}(\xi)$ and $D(\xi)$ are the cofactor and the determinant of the 3×3 matrix with elements $C_{ipjq}\xi_p\xi_q$ respectively ($\xi^2 = \xi_i\xi_i$, $\bar{\xi} = \xi/\xi$). Since $N_{ij}(\xi)$ and $D(\xi)$ are homogeneous polynomials of the 4th and 6th orders respectively, the above form, on integration with respect to ξ, becomes

$$u_i(\mathrm{x}) = -(8\pi^2)^{-1} \frac{\partial}{\partial x_l} \int_\Omega d\mathrm{x}' \int_{S^2} C_{jlmn} \varepsilon^*_{mn}(\mathrm{x}')(N_{ij}(\bar{\xi})/D(\bar{\xi}))\delta(\bar{\xi}\cdot(\mathrm{x}-\mathrm{x}'))\, dS(\bar{\xi}), \quad (2)$$

where δ is the Dirac delta function.

When Ω is an ellipsoidal domain with associated principal axes a_1, a_2, a_3, the following transformation employed by ASARO and BARNETT [39] is useful:

$$\left.\begin{aligned} x_1/a_1 = y_1, \quad x_2/a_2 = y_2, \quad x_3/a_3 = y_3, \\ x'_1/a_1 = y'_1, \quad x'_2/a_2 = y'_2, \quad x'_3/a_3 = y'_3, \\ a_1\bar{\xi}_1 = \zeta_1, \quad a_2\bar{\xi}_2 = \zeta_2, \quad a_3\bar{\xi}_3 = \zeta_3, \\ \zeta_1/\zeta = \bar{\zeta}_1, \quad \zeta_2/\zeta = \bar{\zeta}_2, \quad \zeta_3/\zeta = \bar{\zeta}_3, \\ \zeta = (\zeta_1^2+\zeta_2^2+\zeta_3^2)^{\frac{1}{2}} = \{(a_1\bar{\xi}_1)^2+(a_2\bar{\xi}_2)^2+(a_3\bar{\xi}_3)^2\}^{\frac{1}{2}}. \end{aligned}\right\} \quad (3)$$

In the above transformation, the rectangular cartesian coordinate system has been taken along the principal axes directions of the ellipsoid. If the coordinate system is taken in arbitrary orientation, then (3) still holds for the components of the vectors x, y, $\bar{\xi}$, $\bar{\zeta}$ in the principal axes directions of the ellipsoid.

If x lies within the ellipsoid, then (2), with use of (3), can be written as

$$u_i(\mathrm{x}) = -(a_1a_2a_3/8\pi^2) \frac{\partial}{\partial x_l} \int_0^R r\, dr \int_0^{2\pi} d\varphi \int_{S^2} C_{jlmn} \varepsilon^*_{mn}(\mathrm{y}')(N_{ij}(\bar{\xi})/\zeta D(\bar{\xi}))\, dS(\bar{\xi}), \quad (4)$$

where

$$\left.\begin{aligned} R = \{1-(\mathrm{x}\cdot\bar{\xi})^2/\zeta^2\}^{\frac{1}{2}}, \\ \mathrm{y}' = (\mathrm{y}\cdot\bar{\zeta})\bar{\zeta} + r(\mathrm{m}\cos\varphi + \mathrm{n}\sin\varphi), \end{aligned}\right\} \quad (5)$$

and φ, m, n are shown in Fig. 1. Here, m and n are orthogonal unit vectors in the plane $\xi\cdot(y-y')=0$, r is the distance between the point y′ and the point of intersection of ξ with the plane $\xi\cdot(y-y')=0$, and φ is the angle between r and m.

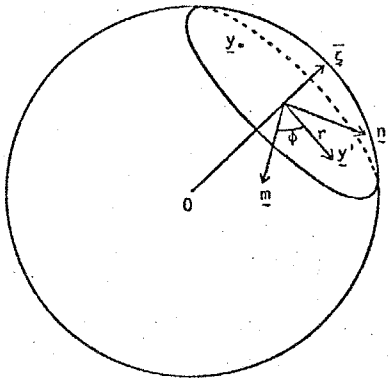

FIG. 1. Illustration of the domain of integration with respect to r, φ for equation (4).

Let us consider the case when

$$\varepsilon^*_{nm}(y') = \bar{\varepsilon}^*_{nm}\exp(ic_p x'_p/a_p) = \bar{\varepsilon}^*_{nm}\exp(ic_p y'_p), \tag{6}$$

where $\bar{\varepsilon}^*_{nm}$ is constant. Since y′ is a function of φ and r (through the second term in the right side of (5_2), the integrals with respect to φ and r in (4) can easily be found. Before integration, however, $c_p y'_p$ is rewritten as follows (see Fig. 2):

$$\begin{aligned} c_p y'_p &= (y\cdot\xi)(c\cdot\xi)+r\{(c\cdot m)\cos\varphi+(c\cdot n)\sin\varphi\} \\ &= (x\cdot\xi)c_p a_p\xi_p/\zeta^2 + rc_0\cos(\varphi-\alpha), \end{aligned} \tag{7}$$

where

$$\left.\begin{aligned} c_0 &= \{c_p c_p-(c_p a_p\xi_p/\zeta)^2\}^{\frac{1}{2}}, \\ (c\cdot m)/c_0 &= \cos\alpha, \qquad (c\cdot n)/c_0 = \sin\alpha. \end{aligned}\right\} \tag{8}$$

Since

$$\left.\begin{aligned} \int_0^{2\pi}\exp\{irc_0\cos(\varphi-\alpha)\}\,d\varphi &= 2\pi J_0(c_0 r), \\ \{zJ_1(z)\}' &= zJ_0(z), \end{aligned}\right\} \tag{9}$$

where J_0, J_1 are the Bessel functions of the first kind of the zeroth and first orders respectively, we can write (4) as

$$u_i(x) = -(a_1 a_2 a_3/4\pi)C_{jlmn}\bar{\varepsilon}^*_{nm}\frac{\partial}{\partial x_l}\int_{S^2} c_0^{-1}RJ_1(c_0R)\exp\{i(x\cdot\xi)c_p a_p\xi_p/\zeta^2\}\times \times(N_{ij}(\xi)/\zeta D(\xi))\,dS(\xi), \tag{10}$$

where R is defined in (5).

After differentiation with respect to x_l, we have finally

$$u_i(x) = (a_1 a_2 a_3/4\pi)C_{jlmn}\bar{\varepsilon}^*_{nm}\int_{S^2}\{(x\cdot\xi)J_0(c_0R)-ic_p a_p\xi_p RJ_1(c_0R)/c_0\}\times \times\exp\{i(x\cdot\xi)c_p a_p\xi_p/\zeta^2\}(\xi_l N_{lj}(\xi)/\zeta^3 D(\xi))\,dS(\xi). \tag{11}$$

The solution (11) is called the *fundamental* solution. When ε^*_{nm} is given as an arbitrary function, it can be expressed by its Fourier series or integral in terms of (6). The corresponding solution for u_i is the summation or integration of (11) with respect to appropriate values of c.

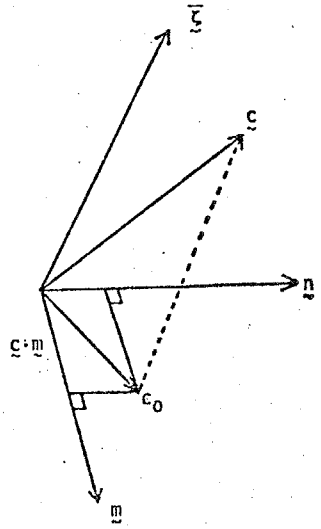

FIG. 2. Definition of c_0 and the relation of c to other vectors m, n, $\bar{\zeta}$.

APPENDIX B

Flat Ellipsoidal Inclusion

When one of the principal axes of the ellipsoidal inclusion (say a_3) becomes zero, then the expression (11) is much simplified.

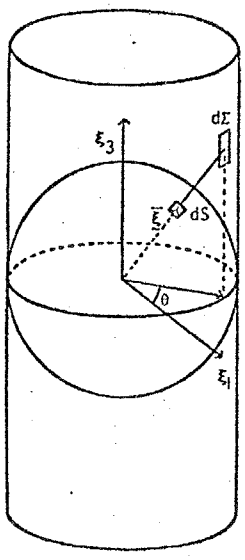

FIG. 3. Transformation of the surface of the unit sphere S^2 into the surface of the enveloping cylinder.

The unit sphere S^2 is transformed into the cylinder as shown in Fig. 3. Then, the cylinder surface element $d\Sigma$ is $d\theta\, d\xi_3$ which is related to dS by

$$dS(\bar{\xi}) = d\theta\, d\xi_3/(1+\xi_3^2)^{\frac{1}{2}}. \tag{13}$$

Also,

$$\bar{\xi}_1 = \cos\theta/(1+\xi_3^2)^{\frac{1}{2}}, \qquad \bar{\xi}_2 = \sin\theta/(1+\xi_3^2)^{\frac{1}{2}}, \qquad \bar{\xi}_3 = \xi_3/(1+\xi_3^2)^{\frac{1}{2}}, \tag{14}$$

and

$$\zeta^{-3}\, dS(\bar{\xi}) = (a_1^2\cos^2\theta + a_2^2\sin^2\theta + a_3^2\xi_3^2)^{-\frac{1}{2}}\, d\theta\, d\xi_3, \tag{15}$$

where $-\infty \leqslant \xi_3 \leqslant +\infty$.

With use of the identity

$$(a_1^2\cos^2\theta + a_2^2\sin^2\theta + a_3^2\xi_3^2)^{-\frac{1}{2}} = (a_1^2\cos^2\theta + a_2^2\sin^2\theta)^{-1} \times$$
$$\times \frac{\partial}{\partial\xi_3}\{\xi_3/(a_1^2\cos^2\theta + a_2^2\sin^2\theta + a_3^2\xi_3^2)^{\frac{1}{2}}\}, \tag{16}$$

then by integration of (11) by parts with respect to ξ_3,

$$u_i(\mathrm{x}) = (a_1 a_2 a_3/4\pi) C_{jlmn}\bar{\varepsilon}^*_{nm} \int_0^{2\pi} d\theta [\{(\mathrm{x}\cdot\bar{\xi})J_0(c_0R) - ic_p a_p \bar{\xi}_p R J_1(c_0R)/c_0\} \times$$
$$\times \exp\{i(\mathrm{x}\cdot\bar{\xi})c_p a_p \bar{\xi}_p/\zeta^2\}(\bar{\xi}_l N_{ij}(\bar{\xi})/D(\bar{\xi}))]_{\xi_3=\infty}(2/a_3)/(a_1^2\cos^2\theta + a_2^2\sin^2\theta) -$$
$$-(a_1 a_2 a_3/4\pi) C_{jlmn}\bar{\varepsilon}^*_{nm} \int_0^{2\pi} d\theta \int_{-\infty}^{\infty} \xi_3 (a_1^2\cos^2\theta + a_2^2\sin^2\theta)^{-1} \times$$
$$\times (a_1^2\cos^2\theta + a_2^2\sin^2\theta + a_3^2\xi_3^2)^{-\frac{1}{2}} \frac{\partial}{\partial\xi_3}[\{(\mathrm{x}\cdot\bar{\xi})J_0(c_0R) -$$
$$- ic_p a_p \bar{\xi}_p R J_1(c_0R)/c_0\} \exp\{i(\mathrm{x}\cdot\bar{\xi})c_p a_p \bar{\xi}_p/\zeta^2\}(\bar{\xi}_l N_{ij}(\bar{\xi})/D(\bar{\xi}))]\, d\xi_3. \tag{17}$$

For $\xi_3 \to \infty$, from (14),

$$\bar{\xi}_1 = 0, \qquad \bar{\xi}_2 = 0, \qquad \bar{\xi}_3 = 1, \tag{18}$$

and therefore

$$\left.\begin{aligned}(\mathbf{x}\cdot\bar{\xi}) &= x_3, \qquad \zeta = a_3,\\ c_0 &= (c_1^2+c_2^2)^{\frac{1}{2}}, \qquad R = (1-x_3^2/a_3^2)^{\frac{1}{2}}.\end{aligned}\right\} \tag{19}$$

Furthermore, for $a_3 \to 0$, the second integral in the right side of (17) vanishes, and (17) becomes

$$u_i(\mathbf{x}) = C_{jlmn}\bar{\varepsilon}^*_{nm}x_3 J_0(c_0R)\exp(ix_3c_3/a_3)\bar{\xi}_l N_{ij}(\bar{\xi})D^{-1}(\bar{\xi}), \tag{20}$$

where use has been made of the result

$$\int_0^{2\pi}(a_1^2\cos^2\theta + a_2^2\sin^2\theta)^{-1}\,d\theta = 2\pi/a_1a_2 \tag{21}$$

and $\bar{\xi}$, c_0, R are defined in (18) and (19).

Since we are considering a point $\mathbf{x}$ inside the inclusion, setting $x_3 = 0$ before taking the limit $a_3 \to 0$ can be justified. Then, (20) leads to

$$u_i(x) = 0. \tag{22}$$

By taking the derivative of (20) with respect to x_k, we obtain the expressions for the total strain and, therefore, also for the stress components throughout the inclusion:

$$\left.\begin{aligned}u_{i,k} &= C_{jlmn}\bar{\varepsilon}^*_{nm}J_0(c_0)\bar{\xi}_k\bar{\xi}_l N_{ij}(\bar{\xi})D^{-1}(\bar{\xi}),^{\dagger}\\ \sigma_{pq} &= C_{pqik}[C_{jlmn}\bar{\varepsilon}^*_{nm}J_0(c_0)\bar{\xi}_k\bar{\xi}_l N_{ij}(\bar{\xi})D^{-1}(\bar{\xi}) - \bar{\varepsilon}^*_{kl}\exp\{i(c_1x_1/a_1 + c_2x_2/a_2)\}],\end{aligned}\right\} \tag{23}$$

where $\bar{\xi}$ is the unit vector normal to the surface of the ellipse. When the coordinate system is taken along the principal axes of the ellipse, $\bar{\xi}$ is given by (18). On comparison with the solution for the uniform eigenstrain throughout the inclusion (KINOSHITA and MURA, [20]), the effect of the periodic distribution of eigenstrain on the total distortion appears by the presence of the factor $J_0(c_0)$. It is interesting to note that all the total strain components vanish for a periodic distribution of eigenstrain satisfying

$$J_0(c_0) = 0. \tag{24}$$

When ε^*_{nm} is constant ($c_p \to 0$) in an extremely-flat ellipsoidal inclusion ($a_3 \to 0$), (23) becomes

$$\sigma_{pq} = C_{pqi3}C_{j3mn}\varepsilon^*_{nm}N_{ij}(\bar{\xi})D^{-1}(\bar{\xi}) - C_{pqik}\varepsilon^*_{ki} \tag{25}$$

since $J_0(0) = 1$. By definition, we have

$$C_{pqik}\bar{\xi}_q\bar{\xi}_k N_{ij}(\bar{\xi})D^{-1}(\bar{\xi}) = \delta_{pj}. \tag{26}$$

where δ_{pj} is the Kronecker delta. When (18) is satisfied, (26) is identical to

$$C_{p3i3}N_{ij}(\bar{\xi})D^{-1}(\bar{\xi}) = \delta_{pj}. \tag{27}$$

From (27) and (25), it is known that

$$\sigma_{p3} = 0, \tag{28}$$

as should be expected for the case of a very flat inclusion. Further, from (23),

$$u_{i,3} = C_{j3m1}\varepsilon^*_{1m}N_{ij}(\bar{\xi})D^{-1}(\bar{\xi}) + C_{j3m2}\varepsilon^*_{2m}N_{ij}(\bar{\xi})D^{-1}(\bar{\xi}) + C_{j3m3}\varepsilon^*_{3m}N_{ij}(\bar{\xi})D^{-1}(\bar{\xi}). \tag{29}$$

If

$$\varepsilon^*_{11} = \varepsilon^*_{22} = \varepsilon^*_{12} = 0, \tag{30}$$

---

† It can be shown from (18) and (23) that

$$u_{i,1} = u_{i,2} = 0\ .$$

then it may be shown from (27) and (29) that

$$\tfrac{1}{2}(u_{1,3}+u_{3,1}) = \varepsilon^*_{13}, \qquad \tfrac{1}{2}(u_{2,3}+u_{3,2}) = \varepsilon^*_{23}, \qquad u_{3,3} = \varepsilon^*_{33},\dagger \tag{31}$$

and all the stress components vanish, *i.e.*

$$\sigma_{pq} = 0, \tag{32}$$

resulting, of course, in vanishing elastic strain energy. Further, the arbitrary vector parallel to the flat surface does not change, since $u_{i,1} = u_{i,2} = 0$ from (23). This result is equivalent to the postulate tacitly assumed in the phenomenological theory of martensitic transformation (see, *e.g.*, WAYMAN [45]).

---

† Since $u_{i,1} = u_{i,2} = 0$, (31) can be written as

$$u_{1,3} = 2\varepsilon^*_{13}\ ,\ u_{2,3} = 2\varepsilon^*_{23}\ ,\ u_{3,3} = \varepsilon^*_{33}\ .$$

APPENDIX C

Making an Arbitrary Plane as a Habit Plane by Postulating Three Kinds of Lattice Invariant Shears in the Calculation Based on Phenomenological Theory

Two different ways — infinitesimal and finite deformation approaches — will be taken in the following.

i) Infinitesimal deformation approach

Consider n kinds of independent shears as lattice invariant deformations. Let the transformation strain be ε^T_{ij} and the plastic strain caused by the k-th shear system $m(k)\varepsilon^P_{ij}(k)$, where m(k) is an unknown amount of the shear to be determined and $\varepsilon^P_{ij}(k)$ is a crystallographically determined shear strain in the k-th shear system. Thus, the total eigenstrain accompanying the transformation can be written as

$$\varepsilon^*_{ij} = \varepsilon^T_{ij} + \sum_{k=1}^{n} m(k)\varepsilon^P_{ij}(k) \ . \tag{A.1}$$

If the coordinate axes are chosen to be parallel to the principal axes of a flat ellipsoid (3.9), the necessary and sufficient condition to make x_3 axis as the habit plane normal is (see equation (3.13))

$$\varepsilon^*_{11} = \varepsilon^*_{22} = \varepsilon^*_{12} = 0 \tag{A.2}$$

that is,

$$\begin{aligned} \varepsilon^*_{11} &= \varepsilon^T_{11} + \sum_{k=1}^{n} m(k)\varepsilon^P_{11}(k) = 0 \ , \\ \varepsilon^*_{22} &= \varepsilon^T_{22} + \sum_{k=1}^{n} m(k)\varepsilon^P_{22}(k) = 0 \ , \\ \varepsilon^*_{12} &= \varepsilon^T_{12} + \sum_{k=1}^{n} m(k)\varepsilon^P_{12}(k) = 0 \ . \end{aligned} \tag{A.3}$$

In these three equations, ε^T_{ij} and $\varepsilon^P_{ij}(k)$ $(k = 1, \cdots, n)$ are constants depending on and determined by the direction of the x_3-axis of the flat ellipsoid.

As is well known, the maximum number of the independent shear system is five. Furthermore, in F.C.C., B.C.C. and H.C.P. structures, there exist in fact five independent shear systems, including twinning systems. Let us choose any arbitrary five shear systems, $\varepsilon^P_{ij}(1), \cdots, \varepsilon^P_{ij}(5)$. It can be proved that out of the five shear systems there exists at least one combination of the

three shear systems, which satisfy

$$\begin{vmatrix} \varepsilon^{P}_{11}(1) & \varepsilon^{P}_{11}(2) & \varepsilon^{P}_{11}(3) \\ \varepsilon^{P}_{22}(1) & \varepsilon^{P}_{22}(2) & \varepsilon^{P}_{22}(3) \\ \varepsilon^{P}_{12}(1) & \varepsilon^{P}_{12}(2) & \varepsilon^{P}_{12}(3) \end{vmatrix} \neq 0 \ . \qquad (A.4)$$

If one uses these three systems, thus letting $n = 3$ in (A.3), one can solve (A.3) with respect to $m(k)$. In other words, with a choice of the three shear systems, of which the vectors, $[\varepsilon^{P}_{11}(k), \ \varepsilon^{P}_{22}(k), \ \varepsilon^{P}_{12}(k)]$, are independent of each other and the existence of which is assured, one can have any arbitrary plane being the habit plane of a thin plate martensite.

ii) Finite deformation approach

Here, the discussion based on the Wechsler-Lieberman-Read theory[5] will be given.

By adopting the n kinds of lattice invariant deformations, the total shape deformation of the martensitic transformation T (invariant plane deformation) can be factorized into 3×3 matrices of rigid body rotation R, lattice deformation B and n kinds of lattice invariant shear deformations $P(k)$ ($k = 1, \cdots, n$) as

$$T = RBP(1)P(2)\cdots P(n) \ . \qquad (A.5)$$

In (A.5), $P(k)$ is a matrix expressing the pure shear deformation of the k-th system and can be written as

$$P(k) = I + m(k)\underset{\sim}{d}(k)\underset{\sim}{p}'(k) \qquad (\underset{\sim}{p}'(k)\underset{\sim}{d}(k) = 0) \qquad (A.6)$$

where I is the unit 3×3 matrix, $m(k)$ is an unknown amount of the shear and $\underset{\sim}{d}(k)$ and $\underset{\sim}{p}(k)$ are unit vectors representing the shear direction and the shear plane normal of the k-th shear system, respectively. Vectors without and with a prime such as $\underset{\sim}{d}(k)$ and $\underset{\sim}{p}'(k)$ indicate the column and the row vectors, respectively. For the saving of the space, the column and the row vectors are distinguished by using different types of parentheses in writing down their components such as $\underset{\sim}{d}(k) = [d(k)_1, d(k)_2, d(k)_3]$ and $\underset{\sim}{p}'(k) = (p(k)_1, p(k)_2, p(k)_3)$. From these notations, $\underset{\sim}{d}(k)\underset{\sim}{p}'(k)$ becomes a matrix whose (i,j) component is $d(k)_i p(k)_j$ and $\underset{\sim}{p}'(k)\underset{\sim}{d}(k)$ becomes a scalar product of the vectors $\underset{\sim}{p}(k)$ and $\underset{\sim}{d}(k)$.

Putting F as

$$F = BP(1)P(2)\cdots P(n) \ , \qquad (A.7)$$

F must be an undistorted plane deformation with m(k) (k = 1,$\cdots$, n) as unknown parameters.

If the coordinate axes are chosen to be parallel to the parent crystalline axes and if one wishes $\underset{\sim}{h} = [\, h_1,\ h_2,\ h_3]$ as an undistorted plane normal, it is necessary and sufficient that two vectors normal to $\underset{\sim}{h}$, i.e., $\underset{\sim}{u}$ and $\underset{\sim}{v}$, which are not parallel to each other, do not change their lengths and that the scalar product of them remains unchanged before and after the operation of F[5]. This situation can be written as

$$\begin{aligned} \underset{\sim}{u}'F'F\underset{\sim}{u} &= \underset{\sim}{u}'\underset{\sim}{u} \\ \underset{\sim}{v}'F'F\underset{\sim}{v} &= \underset{\sim}{v}'\underset{\sim}{v} \\ \underset{\sim}{u}'F'F\underset{\sim}{v} &= \underset{\sim}{u}'\underset{\sim}{v} \end{aligned} \qquad \text{(A.8)}$$

where F' denotes the transposed matrix of F.

As F'F contains m(k) (k = 1,$\cdots$, n), (A.8) constitutes a simultaneous equation system with respect to m(k). Thus one can solve (A.8) by postulating as many as three unknown parameters, m(1), m(2) and m(3), i.e., n = 3.

iii) Example of the analyses

For simplicity and convenience, the derivation of $\{112\}_f$ habit plane found in α-martensite in stainless steels will be shown. This type of the habit plane was discussed by Kelly[16] introducing so-called 'dilatation parameter' in the phenomenological calculation.

Let the three independent shear systems be $(\bar{1}01)_f[101]_f$, $(1\bar{1}1)_f[011]_f$ and $(111)_f[\bar{1}\bar{1}2]_f$. The first system is identical to that in the original phenomenological theory and corresponds to the $\{211\}_b\langle 111\rangle_b$ type of B.C.C. twinning shear system in the martensite. The second is the normal slip system in the F.C.C. phase and the third is the one which was introduced in the calculation by Kelly[16].

Matrices B, P(1), P(2) and P(3) are written in the parent crystalline coordinate axes as

$$B = \begin{pmatrix} \eta_1 & 0 & 0 \\ 0 & \eta_1 & 0 \\ 0 & 0 & \eta_2 \end{pmatrix}, \qquad \text{(A.9)}$$

$$P(1) = \begin{pmatrix} 1-m(1)/2 & 0 & m(1)/2 \\ 0 & 1 & 0 \\ -m(1)/2 & 0 & 1+m(1)/2 \end{pmatrix}, \qquad \text{(A.10)}$$

$$P(2) = \begin{pmatrix} 1 & 0 & 0 \\ m(2)/\sqrt{6} & 1-m(2)/\sqrt{6} & m(2)/\sqrt{6} \\ m(2)/\sqrt{6} & -m(2)/\sqrt{6} & 1+m(2)/\sqrt{6} \end{pmatrix}, \qquad (A.11)$$

$$P(3) = \begin{pmatrix} 1-m(3)/3\sqrt{2} & -m(3)/3\sqrt{2} & -m(3)/3\sqrt{2} \\ -m(3)/3\sqrt{2} & 1-m(3)/3\sqrt{2} & -m(3)/3\sqrt{2} \\ 2m(3)/3\sqrt{2} & 2m(3)/3\sqrt{2} & 1+2m(3)/3\sqrt{2} \end{pmatrix}. \qquad (A.12)$$

In order to make $(\bar{2}11)_f$ plane as a habit plane, two vectors in the habit plane, say $\underset{\sim}{u} = [\ 0, -1, 1\ ]_f$ and $\underset{\sim}{v} = [\ 1, 1, 1\ ]_f$, must satisfy the three equations in (A.8). By using a computer together with the values $\eta_1 = 1.1321$ and $\eta_2 = 0.8005$[45], it is shown that (A.8) can be satisfied with m(k) given by

$$\begin{aligned} m(1) &= 0.2918 \\ m(2) &= -0.0073 \quad \text{(large deformation approach)} \\ m(3) &= 0.1022 \end{aligned} \qquad (A.13)$$

In the infinitesimal deformation approach discussed in i), simple calculation using (A.3) gives the results as

$$\begin{aligned} m(1) &= 0.3103 \\ m(2) &= -0.0794 \quad \text{(infinitesimal deformation approach)} \\ m(3) &= 0.1346 \end{aligned} \qquad (A.14)$$

In addition, it is quite matter-of-course that in the present case of the $(\bar{2}11)_f$ habit plane, the orientation relationship between the parent phase and the martensite is exactly the Kurdjumov-Sachs relationships described as $(111)_f // (110)_b$ and $[0\bar{1}1]_f // [\bar{1}11]_b$ (variant 1-2 in Table 2.1 (p.12)). For, both the $[111]_f$ and the $[0\bar{1}1]_f$ directions, which correspond respectively to $[110]_b$ and $[\bar{1}11]_b$ from the Bain correspondence, lie on the $(\bar{2}11)_f$ habit plane and, thus, they are actually invariant (undistorted and unrotated) directions before and after the martensitic transformation.

Thus, we can obtain $(\bar{2}11)_f$ habit plane and the K-S orientation relationship by postulating three independent shear deformations in place of the dilatation parameter, the physical meaning of which is vaguely defined, and one shear deformation introduced by Kelly[16].

In a similar manner, one can, of course, obtain any other plane as a habit plane by introducing three independent shear deformations in the phenomenological calculation.

REFERENCES

[1] A. J. Bogers, Acta Met. 10, 260 (1962).

[2] G. H. Olsen and W. A. Jesser, Acta Met. 19, 1009 (1971).

[3] Y. Higo, F. Lecroisey and T. Mori, Acta Met. 22, 313 (1974).

[4] G. Stone and G. Thomas, Met. Trans. 5, 2095 (1974).

[5] M. S. Wechsler, D. S. Lieberman and T. A. Read, Trans. AIME 197, 1503 (1953).

[6] J. S. Bowles and J. K. Mackenzie, Acta Met. 2, 129, 138, 224 (1954).

[7] J. R. Patel and M. Cohen, Acta Met. 1, 531 (1953).

[8] J. W. Christian, The Theory of Transformation in Metals and Alloys. Pergamon Press, Oxford (1965).

[9] D. Goodchild, W. T. Roberts and D. V. Wilson, Acta Met. 18, 1137 (1970).

[10] H. Onodera, H. Goto and I. Tamura, Proc. First Japan Inst. Metals Int. Symp. Kobe (1976) p.327.

[11] G. F. Bolling and R. H. Richman, Scripta Met. 4, 539 (1970).

[12] G. H. Olsen and W. A. Jesser, Acta Met. 19, 1299 (1971).

[13] A. J. Bogers and W. G. Burgers, Acta Met. 12, 255 (1964).

[14] N. D. H. Ross and A. G. Crocker, Acta Met. 18, 405 (1970).

[15] D. P. Dunne and C. M. Wayman, Acta Met. 19, 425 (1971).

[16] P. M. Kelly, Acta Met. 13, 635 (1965).

[17] T. Mura, T. Mori and M. Kato, J. Mech. Phys. Solids 24, 305 (1976).

[18] J. D. Eshelby, Proc. Roy. Soc. A241, 376 (1957).

[19] J. D. Eshelby, Proc. Roy. Soc. A252, 561 (1959).

[20] N. Kinoshita and T. Mura, phy. stat. sol. (a)5, 759 (1971).

[21] T. Mura and P. C. Cheng, to appear in J. Appl. Mech.

[22] Y. Higo, Dr. Eng. Dissertation, Tokyo Institute of Technology, Tokyo (1974).

[23] M. Kato, Master Eng. Dissertation, Tokyo Institute of Technology, Tokyo (1975).

[24] J. A. Klostermann and W. G. Burgers, Acta Met. 12, 355 (1964).

[25] W. G. Burgers and J. A. Klostermann, Acta Met. 13, 568 (1965).

[26] J. F. Breedis and W. D. Robertson, Acta Met. 11, 547 (1963).

[27] G. F. Bolling and R. H. Richman, Phil. Mag. 19, 247 (1969); Acta Met. 18, 673 (1970).

[28] T. Maki, Y. Tomota and I. Tamura, J. Japan Inst. Metals 38, 871 (1974).

[29] T. Suzuki, H. Kojima, K. Suzuki, T, Hashimoto, S. Koike and M. Ichihara, Scripta Met. 10, 353 (1976).

[30] M. F. Ashby, Phil. Mag. 21, 399 (1970).

[31] G. Kurdjumov and G. Sachs, Zeits. f. Phys. 64, 325 (1930).

[32] Z. Nishiyama, Sci. Rep. Tohoku Univ. 23, 637 (1934).

[33] S. Dash and N. Brown, Acta Met. 14, 595 (1966).

[34] R. P. Reed and R. E. Schramm, J. Appl. Phys. 40, 3453 (1969).

[35] J. D. Eshelby, Progress in Solid Mechanics (edited by Sneddon and Hill), 2, North-Holland, Amsterdam (1961) p.89.

[36] L. J. Walpole, Proc. Roy. Soc. A300, 270 (1967).

[37] J. R. Willis, The solution of Asymmetric Problem of Elasticity by Fourier Transforms. Cambridge University, Adams Prize Essay (unpublished) (1970).

[38] G. P. Sendeckyji, Ph.D. Dissertation, Northwestern University, Evanston, Illinois (1967).

[39] R. J. Asaro and D. M. Barnett, J. Mech. Phys. Solids 23, 77 (1975).

[40] I. Tamura, H. Yoshimura, M. Ibaraki and M. Tagaya, Trans. J. Inst. Metals 5, 47 (1964).

[41] K. E. Easterling and H. M. Miekk-oja, Acta Met. 15, 1133 (1967).

[42] M. Shibata and K. Ono, Acta Met. 23, 587 (1975).

[43] M. Shibata and K. Ono, Acta Met. 25, 35 (1977).

[44] K. R. Kinsman, J. W. Sprys and R. J. Asaro, Acta Met. 23, 1431 (1975).

[45] C. M. Wayman, Introduction to the Crystallography of Martensitic Transformations, Macmillan, New York (1964).

[46] K. E. Easterling and A. R. Thölén, Acta Met 24, 333 (1976).

[47] Z. Nishiyama, Martensitic Transformations (Fundamental Volume) (in Japanese), Maruzen, Tokyo (1971).

[48] S. Kajiwara and W. S. Owen, Scripta Met. 11, 137 (1977).

[49] D. R. Clarke, Met. Trans. 7A, 723 (1976).

[50] J. B. Newkirk, Trans. AIME 209, 1214 (1957).

[51] G. R. Woolhouse, Phil. Mag. 28, 65 (1973).

[52] K. Matsuura, M. Tsukamoto and K. Watanabe, Acta Met. 21, 1033 (1973).

[53] K. E. Easterling and G. C. Weatherly, Acta Met. 17, 845 (1969).

[54] V. Vítek, Scripta Met. 4, 725 (1970).

[55] K. Masuda, private communication.

[56] F. R. N. Nabarro, Proc Roy Soc. A175, 519 (1940).

[57] F. Laszlo, J. Iron Steel Inst. 164, 5 (1950).

[58] J. K. Lee, D. M. Barnett and H. I. Arronson, Met. Trans. 8A, 963 (1977).

[59] K. Salma and G. A. Alers, J. Appl. Phys. 39, 4857 (1968).

[60] N. Kikuchi, J. Japan Inst. Metals 35, 518 (1971).

ACKNOWLEDGEMENTS

Since I first came into contact with Prof. Tsutomu Mori, my advisor, five years ago, my way of living has changed martensitically. He opened my eyes both inside and outside of my research work. However, once I would express my sincere gratitude to him enough, it must become as long as this thesis. Thus, I cannot help giving up to write it down here.

Thanks are also due to Prof. Akikazu Sato, my advisor, who gave me experimental advice and useful discussions. The help of Dr. Kin-ichi Masuda as a scientist and, sometimes, as a colleague is much acknowledged.

Other persons to whom I owe this thesis are as follows :

Prof. Tadahisa Nakamura,
Mr. Shirō Horie,
Mr. Takehiko Eto,
Mr. Yoshinori Sunaga,
Dr. Hideki Morikawa,
Mr. Hideo Umezawa,
Mr. Ryoichi Monzen,
Mr. Toshiyuki Miyazaki,
Dr. Yakichi Higo,
Dr. Yū Murakami,
Prof. Toshio Mura (Northwestern University),
Dr. Setsuo Kajiwara (National Research Inst. for Metals),
Mr. Toshihisa Ishikawa (Fujitsu Ltd.),
Mr. Manabu Yoshimura (University of Tokyo),
Prof. Zenji Nishiyama (Nippon Steel Corp.),
Prof. Imao Tamura (Kyoto University),
Prof. W. G. Burgers (the Netherlands).

December, 1977

加藤雅治

Masaharu Kato